ISTANBUL TECHNICAL UNIVERSITY ★ GRADUATE SCHOOL

ELECTRO OPTICAL PROPERTIES OF LIQUID CRYSTAL NANOCOMPOSITES

Ph.D. THESIS

Mehmet Can ÇETİNKAYA

Department of Physics Engineering

Physics Engineering Programme

DECEMBER 2022

ISTANBUL TECHNICAL UNIVERSITY ★ GRADUATE SCHOOL

ELECTRO OPTICAL PROPERTIES OF LIQUID CRYSTAL NANOCOMPOSITES

Ph.D. THESIS

Mehmet Can ÇETİNKAYA
(509132102)

Department of Physics Engineering

Physics Engineering Programme

Thesis Advisor: Prof. Dr. Sevtap YILDIZ ÖZBEK

DECEMBER 2022

İSTANBUL TEKNİK ÜNİVERSİTESİ ★ LİSANSÜSTÜ EĞİTİM ENSTİTÜSÜ

SIVI KRİSTAL NANOKOMPOZİTLERİN ELEKTRO-OPTİKSEL ÖZELLİKLERİ

DOKTORA TEZİ

Mehmet Can ÇETİNKAYA
(509132102)

Fizik Mühendisliği Anabilim Dalı

Fizik Mühendisliği Programı

Tez Danışmanı: Prof. Dr. Sevtap YILDIZ ÖZBEK

DECEMBER 2022

Mehmet Can ÇETİNKAYA, a Ph.D. student of ITU Graduate School student ID 509132102 successfully defended the thesis entitled "ELECTRO OPTICAL PROPERTIES OF LIQUID CRYSTAL NANOCOMPOSITES", which he/she prepared after fulfilling the requirements specified in the associated legislations, before the jury whose signatures are below.

Thesis Advisor :	**Prof. Dr. Sevtap YILDIZ ÖZBEK** Istanbul Technical University	.....
Jury Members :	**Prof. Dr.Gönül ERYÜREK** Istanbul Technical University	.....
	Assc. Prof. Dr. Alkan KABAKÇIOĞLU Koç University	.....
	Prof. Dr. Ümit TUNCA Istanbul Technical University	.....
	Assc. Prof. Dr. Bengü ÖZUĞUR UYSAL Kadir Has University	.....

Date of Submission : **29 November 2022**
Date of Defense : **29 December 2022**

To My Beloved Nur

FOREWORD

This thesis was supported by Istanbul Technical University Grant No. 37639, 38206, 40883 and 41101. The author of the thesis received TUBITAK Grant 2214-A in order to study abroad during his PhD. I thank my supervisor Prof. Dr. Sevtap Yıldız Özbek and Prof. Dr. Haluk Özbek for their support and guidance throughout my time in Istanbul Technical University, my father and my mother for raising and supporting me during my long education. Many thanks to my little daughter, Beyza, for making our lives more joyous during the final two and a half years of this thesis. To the love of my life, my wife, my life long companion Nur, I present my deepest gratitude for your patience and support during my PhD. I have drawn my motivation from my love for you, and without it, this thesis could not have been written. Dear Nur, thank you for every day we spent together.

December 2022

Mehmet Can ÇETİNKAYA
(Physics Engineer, M.Sc.)

TABLE OF CONTENTS

ABBREVIATIONS

5CB	**:** Pentylcyanobiphenyl
8CB	**:** Octylcyanobiphenyl
ANL	**:** Analyzer
CNT	**:** Carbon Nanotube
-COOH	**:** Carboxyl group
DSC	**:** Differential scanning calorimetry
ITO	**:** Inidium tin oxide
L	**:** Laser
LC	**:** Liquid crystal
N	**:** Nematic phase
MWCNT	**:** Multi-walled carbon nanotube
LIA	**:** Lock-in amplifier
NR	**:** Nematic range
OSC	**:** Oscilloscope
PC	**:** Computer
PD	**:** Photodiode
PID	**:** Propotional, integral, derivative
POM	**:** Polarization microscopy
POL	**:** Polarizer
QWP	**:** Quarter wave plate
SIG GEN	**:** Signal generator
SmA	**:** Smectic A phase
SWCNT	**:** Single-walled carbon nanotube
T CONT	**:** Temperature controller
wt.%	**:** percentage by weight

SYMBOLS

$\Delta\mathbf{n}$	**:** Birefringence
$\Delta\varepsilon$	**:** Dielectric anisotropy
ε_0	**:** Dielectric permittivity of vacuum
$\mathbf{K_{11}}$	**:** Splay elastic constant
γ	**:** Rotational viscosity
$\mathbf{V}_{th}$	**:** Threshold voltage
$\mathbf{T}$	**:** Temperature
$\mathbf{T}_{NI}$	**:** Nematic to isotropic transition temperature
$\mathbf{T}_{NA}$	**:** Nematic to smectic A transition temperature
$\mathbf{I}_{tr}$	**:** Transmitted light intensity
$\mathbf{I}_0$	**:** Incident light intensity
$\mathbf{C}_{LC}$	**:** Capacitance of liquid crystal filled sample cell
$\mathbf{C}_{empty}$	**:** Capacitance of empty sample cell
$\mathbf{t}_{on}$	**:** Voltage-on response time
$\mathbf{t}_{off}$	**:** Voltage-off response time
$\mathbf{d}$	**:** Sample cell thickness
I	**:** Light intensity
I_0	**:** Intensity of light incident on sample
I_{tr}	**:** Transmitted light intensity
λ	**:** Laser wavelength
ω	**:** Analyzer angular speed
t	**:** Time

LIST OF TABLES

LIST OF FIGURES

ELECTRO OPTICAL PROPERTIES OF LIQUID CRYSTAL NANOCOMPOSITES

SUMMARY

The thesis presents the results of the study on electro-optical and elastic properties of smectogen octylcyanobiphenyl (8CB) liquid crystal doped with well dispersed multi-walled carbon nanotubes (MWCNTs). The study aims to uncover the effect of MWCNT doping on electro-optical properties of smectic liquid crystal 8CB. Nanoparticle doping has been investigated as a possible way to enhance the properties of liquid crystals. Such studies focused on doping nematic liquid crystals have shown that it is possible to increase dielectric anisotropy, lower threshold voltages and increase electrical response times. One of the promising nanoparticles is carbon nanotubes. Carbon nanotubes are exotic materials with very high shape anisotropy. They are basically one atom thick carbon sheets rolled into tubes. If the nanotubes are formed from many cocentric tubes they are called multi-walled carbon nanotubes. Due to their shape anisotropy, they also exhibit anisotropic mechanical and electronic qualities. What makes them especially intriguing to study as liquid crystal dopants is their geometry. Carbon nanotubes are known to produce liquid crystalline dispersions, and once they are dispersed in a liquid crystalline medium, they are expected to impart their anisotropic qualities on this already anisotropic media and enhance them.

The study is carried out on four different samples: one set dispersed with pristine, used as is, MWCNTs of concentrations 0.007 wt.% and 0.07 wt.% (percent by weight), and another set dispersed with -COOH functionalized MWCNTs at same concentrations. So the scope of this thesis is investigating the effects of functionalized and nonfunctionalized MWCNT doping on 8CB liquid crystal host's dielectric anisotropy, threshold voltage, birefringence and response time in Freédericksz transition. Each of said properties were measured against temperature and voltage.

The doping of MWCNTs is carried out by solvent dispersion method. The 8CB and MWCNTs are mixed in high purity toluene. The mixture is heated to 43 °C, where 8CB is in isotropic liquid phase. The mixture is then sonicated and magnetically stirred. Once toluene is evaporated, the remaining 8CB - MWCNT dispersion, or so-called nanocomposite, is filled into sandwich type sample cells by capillary action. Differential scanning calorimetry measurements and polarizing microscopy imaging are also conducted to confirm the existence of nematic and smectic A phases and transition temperatures.

Experimental datum for the temperature dependence of birefringence, dielectric anisotropy, threshold voltage, voltage-on and voltage-off response are presented. Birefringence data is obtained by the rotating analyzer method. Dielectric data is collected by capacitance measurements. Threshold voltages and response times

are obtained by light transmission measurements through crossed polarizers during voltage application on their respective sample cells. The isotropic to nematic and nematic to smectic A phase transition temperatures are obtained from birefringence measurements. The splay elastic constants and rotational viscosities of functionalized and non-functionalized MWCNT dispersed 8CB nanocomposites are calculated from these dielectric anisotropies, threshold voltages and voltage-off response times. The nematic range, temperature interval between isotropic to nematic and nematic to smectic A transition is extended in all nanocomposite samples. Non-functionalized MWCNT nanocomposites have wider nematic ranges than functionalized ones. It is observed that dielectric anisotropies are lowered in all MWCNT dispersed samples, higher concentrations having lower dielectric anisotropies. While birefringence is lowered in pristine MWCNT nanocomposites and functionalized MWCNT 0.07 wt.% nanocomposite, compared to 8CB, functionalized 0.007 wt.% nanocomposite's birefringence is higher than pure 8CB's. These findings suggest that while nematic order is not enhanced with MWCNT dispersions at hand, but the exception, functionalized 0.007 wt.%, points to a possibility of better incorporation of MWCNTs in liquid crystalline media by dispersion of functionalized MWCNTs at low concentrations. The threshold voltages, with the exception of non-functionalized 0.07 wt.%, are increased. Calculation of splay elastic constants (K_{11}) shows that elasticity of the nanocomposites also differ from pure 8CB. The non-functionalized MWCNT nanocomposites have lower elastic constants in the nematic range, while funtionalized MWCNT nanocomposites have higher. Also, a crossover of elastic constants is observed, with respect to temperature, as f0.007 wt.% nanocomposite's elastic constant increases at an higher rate than f0.07 wt.%'s elastic constant. Voltage-on and voltage-off response times are higher in all nanocomposites. Functionalized 0.007 wt.% nanocomposite has the highest voltage-on and voltage-off response times. On the other hand, functionalized 0.07wt.% has the closest response times to 8CB. The calculation of rotational viscosity from response times and elastic constants reveal that rate of change of rotational viscosity with respect to temperature is highest in funtionalized 0.007 wt.% nanocomposite and rotational viscosities of all nanocomposite samples are higher than pure 8CB. With non-functionalized samples, rate of change of rotational viscosity is higher with 0.007 wt.%. Temperature dependencies of rotational viscosity of 0.07 wt.% and pure 8CB are similar. The same is true for functionalized 0.07 wt.%.

The study reveals the temperature dependence of various electro-optical properties of 8CB dispersed with functionalized and non-functionalized MWCNTs. With drops in birefringence and dielectric anisotropy, accompanied by increasing response times and threshold voltages, no electro-optical enhancement is observed in studied samples. However, with effect of functionalization and at optimal concentration, it would be possible to enhance a selected electro-optical property, i.e. improving birefringence while keeping response times at a reasonable level for electrical switching. The results of the study also hint at a complex web of dependencies related to functionalization and concentration, which justifies further numerical and experimental studies on smectic liquid crystal - MWCNT nanocomposites.

SIVI KRİSTAL NANOKOMPOZİTLERİN ELEKTRO-OPTİKSEL ÖZELLİKLERİ

ÖZET

Bu tez, çok duvarlı karbon nanotüpler (MWCNT'ler) ile katkılı smektojen oktilsiyanobifenil (8CB) sıvı kristalin elektro-optik ve elastik özellikleri üzerine yapılmış çalışmanın sonuçlarını sunmaktadır. Çalışma, MWCNT katkılamanın smektik sıvı kristal 8CB'nin elektro-optik özellikleri üzerindeki etkisini ortaya çıkarmayı amaçlamaktadır. Nanoparçacık katkılama, sıvı kristallerin özelliklerini geliştirmenin olası kolay yollarından biri olarak araştırmalara konu olmuştur. Nematik sıvı kristallerin katkılanmasına odaklanılan bu çalışmalarda, dielektrik anizotropiyi arttırmanın, eşik voltajlarını düşürmenin ve elektriksel tepki sürelerini azaltmanın mümkün olduğunu gösterilmiştir. Sıvı kristalin özelliklerini iyileştirmek adına gelecek vaat eden nanoparçacıklardan biri karbon nanotüplerdir. Karbon nanotüpler çok yüksek geometrik anizotropiye sahip egzotik malzemelerdir. Temel olarak, silindir şeklinde sarılmış, bir atom kalınlığında karbon levhaları olarak düşünülebilirler. Nanotüpler birçok eş merkezli silindirden oluşuyorsa, bu nanotüplere çok duvarlı karbon nanotüpler denir. Şekil anizotropilerinden dolayı, anizotropik mekanik ve elektronik nitelikler de sergilerler. Karbon nanotüleri sıvı kristalleri katkılamakta kullanılmasının ana nedeni ve çalışmak için özellikle ilgi çekici yapan şey, geometrileri ile sıvı kristalik düzen arasındaki paralelliktir. Karbon nanotüplerin sıvı kristalik dağınımlar ürettiği bilinmektedir. Aynı zamanda sıvı kristalik bir ortama katkılandıklarında, anizotropik niteliklerinin hali hazırda anizotropik olan sıvı kristal ortama aktararak bu ortamın özelliklerinin anizotropisini arttırmaları beklenmektedir. Bu tez çalışmasında dört farklı karbon nanotüp - sıvı kristal nanokompozit numune konu edilmiştir: Olduğu gibi kullanılan, ağırlıkça % 0.007 ve % 0.07 konsantrasyonlarında MWCNT katkılı 8CB ve yüzeyleri -COOH işlevselleştirilmiş, aynı iki konstrasyonu oluşturacak ağırlıkta MWCNT'ler ile katkılanmış 8CB nanokompozitler. Dolayısıyla bu tezin kapsamı, yüksek ve düşük konsantrasyonda, işlevselleştirilmiş ve işlevselleştirilmemiş MWCNT katkılamanın 8CB sıvı kristal konağın dielektrik anizotropisi, eşik voltajı, çift kırılma ve Freédericksz geçişindeki tepki süresi üzerindeki etkilerini araştırmaktır. Bahsedilen özelliklerin her biri sıcaklık ve örnek hücreye uygulanan voltaja karşı ölçülmüştür.

MWCNT'lerin katkılanması, çözücüde dağınım (solvent dispersion) yöntemiyle gerçekleştirilir. 8CB ve MWCNT'ler yüksek saflıkta toluen içinde karıştırılır. Karışım, 8CB'nin izotropik sıvı fazda olduğu 43 °C'ye ısıtılır. Isıtılan karışım önce sonik banyoda titreşim işlemine tabi tutulur, sonra da manyetik karıştırıcı ile karıştırılır. Bu işlemlere toluen buharlaştırılırken devam edillir. Toluen buharlaştıktan sonra kalan 8CB - MWCNT dağınımı, yani nanokompozit olarak adlandırılan kısım, kılcal etki ile sandviç tipi numune hücrelerine doldurulur. Nematik ve smektik A fazlarının ve geçiş

sıcaklıklarının varlığını doğrulamak için diferansiyel taramalı kalorimetri ölçümleri ve polarize mikroskopi görüntüleme gerçekleştirilir.

Tezde, yukarıda hazırlama yöntemi anlatılan numunelere ait çift kırılmanın, dielektrik anizotropinin, eşik voltajının, voltaj uygulandığındaki ve kaldırıldığındaki tepki sürelerinin sıcaklığa bağlı olarak değişimini gösteren deneysel veriler sunulmaktadır. Çift kırılma verileri, döner analizör yöntemiyle elde edilir. Dielektrik verileri kapasitans ölçümleri ile toplanır. Eşik voltajları ve yanıt süreleri, ilgili numune hücrelerine voltaj uygulaması sırasında çapraz polarizörler aracılığıyla ışık geçirgenliği ölçümleri ile elde edilir. İzotropikten nematiğe ve nematikten smektik A faz geçiş sıcaklıkları çift kırılma ölçümlerinden elde edilir. Numunelerden elde edilen dielektrik anizotropilerden, eşik gerilimlerinden ve gerilim kaldırıldığındaki yanıt sürelerinden işlevselleştirilmiş ve işlevselleştirilmemiş MWCNT dağıtılmış 8CB nanokompozitlerin yayılma elastik sabitleri (splay elastic constant) ve dönel viskoziteleri (rotational viscosity) hesaplanır. Tüm numunelere ait sıcaklığa karşılık çift kırılma verileri incelendiğinde, izotropikten nematiğe ve nematikten smektik A geçişi arasındaki sıcaklık aralığını kapsayan ve nematik aralık olarak adlandırılan sıcaklık aralığının tüm nanokompozit numunelerde büyüdüğü görülür. İşlevselleştirilmemiş MWCNT nanokompozitleri, işlevselleştirilmiş olanlardan daha geniş nematik aralıklara sahiptir. Tüm MWCNT katkılanmış numunelerde dielektrik anizotropinin azaldığı, daha yüksek konsantrasyondakilerin daha düşük dielektrik anizotropiye sahip olduğu gözlemlenmiştir. Saf MWCNT nanokompozitlerde ve ağırlıkça % 0.07 işlevselleştirilmiş MWCNT katkılanmış nanokompozitte çift kırılma saf 8CB'ye kıyasla düşükken, ağırlıkça % 0.007 işlevselleştirilmiş nanokompozitin çift kırılması saf 8CB'ninkinden daha yüksektir. Bu bulgular, eldeki MWCNT katkılı numulerde nematik düzenin artmadığını göstermektedir. Yalnız, ağırlıkça % 0.007 işlevselleştirilmiş MWCNT katkılı nanokompozit istisnası, işlevselleştirilmiş MWCNT'lerin düşük konsantrasyonlarda sıvı kristal ortama daha iyi uyum gösterebilme ihtimalinin mevcut olduğuna işaret etmektedir. İşlevselleştirilmemiş ağırlıkça % 0.07 numune hariç olmak üzere eşik voltajları artmaktadır. Yayılma elastik sabitlerinin (K_{11}) hesaplanması sonucu, nanokompozitlerin esnekliğinin de saf 8CB'den farklı olduğunu görülmektedir. İşlevselleştirilmemiş MWCNT nanokompozitleri, nematik aralıkta daha düşük elastik sabitlere sahipken, işlevselleştirilmiş MWCNT nanokompozitlerin elastik sabitleri daha yüksektir. Ayrıca, işlevselleştirilmiş % 0.007 nanokompozitin elastik sabiti, işlevselliştirilmiş % 0.07'nin elastik sabitinden daha yüksek bir oranda artarken, elastik sabitlerin sıcaklığa bağlı değişim eğrilerinin bir sıcaklıkta birbirlerini kesitiği gözlemlenir. Tüm nanokompozitlerde voltaj açık ve voltaj kapalı yanıt süreleri daha yüksektir. İşlevselleştirilmiş ağırlıkça % 0.007 nanokompozit, en yüksek voltaj açma ve voltaj kapatma yanıt sürelerine sahiptir. Öte yandan, işlevselleştirilmiş ağırlıkça 0.07%, 8CB'ye en yakın yanıt sürelerine sahiptir. Yanıt sürelerinden ve elastik sabitlerden dönel viskozitenin hesaplanması, sıcaklığa göre dönel viskozite sıcaklığa karşılık değişim hızının, işlevselleştirilmiş ağırlıkça % 0.007 katkılı nanokompozitte en yüksek olduğunu ve tüm nanokompozit numunelerin dönel viskozitelerinin saf 8CB'den daha yüksek olduğunu ortaya koymaktadır. İşlevselleştirilmemiş numunelerde, dönel viskozitenin sıcaklıkla değişim oranı ağırlıkça % 0.007 olan numunede daha yüksektir. 0.07 wt.% ve saf 8CB dönme

viskozitesinin sıcaklık bağımlılıkları benzerdir. Aynısı işlevselleştirilmiş ağırlıkça % 0.07 katkılı nanokompozit için de geçerlidir.

Çalışma, işlevselleştirilmiş ve işlevselleştirilmemiş MWCNT'lerle katkılanmış 8CB'nin çeşitli elektro-optik özelliklerinin sıcaklıkla değişimlerini ortaya koymaktadır. Artan tepki süreleri ve eşik voltajlarının eşlik ettiği çift kırılma ve dielektrik anizotropideki düşüşler ile incelenen numunelerde hiçbir elektro-optik iyileştirme gözlenmiştir. Bununla birlikte, işlevselleştirmenin etkisiyle ve optimal konsantrasyonda, seçilen bir elektro-optik özelliği geliştirmek, yani elektriksel anahtarlama için yanıt sürelerini makul bir seviyede tutarken çift kırılmayı iyileştirmek mümkün olabileceği görülmektedir. Çalışmanın sonuçları ayrıca, smektik sıvı kristal - MWCNT nanokompozitleri üzerinde daha fazla sayısal ve deneysel çalışmayı haklı çıkaran işlevselleştirme ve konsantrasyonla ilgili karmaşık bir bağımlılıklar ağına da işaret etmektedir.

1. INTRODUCTION

Liquid crystals (LCs for short) owe their name to their thermodynamically stable phases between an isotropic liquid and a crystalline solid. These phases often exhibit orientational order without or limited long-range positional order. The orientational order results in bulk anisotropy, a variety of physical properties, optical, electrical, mechanical e.g., differ from one chosen axis to another. However, lack of positional order means fluidity and hence the name "liquid crystal". Liquid crystal materials can flow freely and are susceptible to the effects of local or otherwise external fields and forces, which may perturb or entirely reform their present order. Their susceptibility to external stimuli despite retaining some sort of order along with the variety of thermodynamically stable phases makes them appealing for the study of phase transitions as well as applications where direct, low power control of local or bulk properties is desired.

Liquid crystals can either be thermotropic or lyotropic in nature. Thermotropic liquid crystals' phases are determined by temperature, while lyotropic liquid crystal phases are determined by the solvent ratio: Depending on the amount of soluble material added properties of the lyotropic liquid crystalline phase change. Lyotropic LCs have multiple types of constituent molecules, unlike thermotropic LCs. The phase sequence and character of thermotropic liquid crystals are wholly determined by the shape of their molecules and the intermolecular interactions as affected by temperature. [1]

1.1 Two Liquid Crystalline Phases: Nematic and Smectic A

There exist numerous liquid crystal phases but the most common studied liquid crystalline phase is the nematic (N) phase, owing to its simple composition which is easy to study and model. The nematic phase has orientational order along a single axis, either locally or in bulk, which results in anisotropy. The nematic phase is made possible by elongated, rod-like molecules that constitute the liquid crystalline material.

A nematic liquid crystal can easily be aligned in a preferred axis, which is called a "director" by its interaction with a surface. It is optically anisotropic, interacting with the polarization of light passing through, and the director can be reoriented by an electrical field. The nematic liquid crystal alignment can be twisted by arranging aligning surfaces. Various nematic LCs can be mixed to adjust the nematic phase temperature range. All these properties make nematic LCs easy to study, yet versatile enough to be interesting.

Not all liquid crystals completely lack positional order like nematics. Quite the contrary, positional order, however partial, is often encountered in the form of layered formations. The simplest of these is the smectic A (SmA) phase. This phase is characterized by a density modulation along a preferred direction. The layers created by the density modulation contain molecules orientated along the axis of the density modulation. Figure 1.1 shows how the molecules are arranged in N and SmA phases.

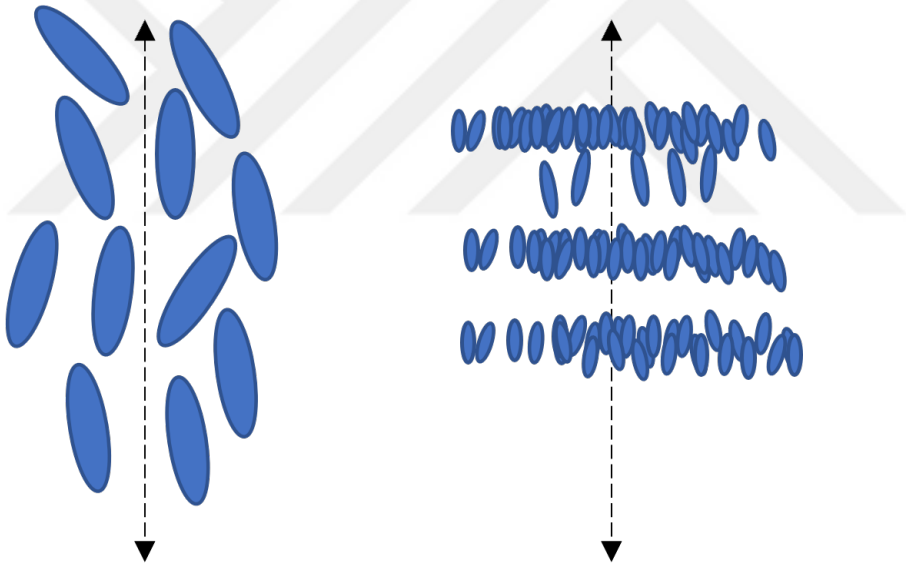

Figure 1.1 : Nematic (left) and Smectic A phases. The arrow lines represent directors.

In each liquid crystalline phase, an order parameter can be defined. For thermotropic LCs, the order parameter conveys the degree to which the liquid crystal is akin to a crystal in the type of order it exhibits. Hence, it is defined so that the order parameter is equal to unity when the average of the order parameter over the bulk is equal to order in an arbitrarily small part of the bulk, and equal to zero at the transition point into the isotropic state. For the nematic phase, it is the normalized coefficient of the second

term of spherical Legendre polynomial expansion, and for the smectic A phase, it is the amplitude of the density wave that forms the layers normalized by average density. Both order parameters decrease as the temperature is increased and equal to zero as the phase vanishes.

1.2 Electro - Optic Properties

The order parameter of a liquid crystalline phase is often directly associated with various anisotropic physical quantities. The dielectric constant is one such quantity. Dielectric anisotropy of a liquid crystal causes optical anisotropy, the birefringence. The light wave polarized parallel to the director and polarized perpendicular to the director propagates through different refractive indexes. Linearly polarized light is polarized at an intermediate angle director and the axis perpendicular to the director experiences retardation in the axis of one component and becomes elliptically polarized. This fact is exploited in order to study the order of the birefringent liquid crystals, such as nematics, by using crossed polarizers.

The dielectric anisotropy of a liquid crystal affects its electromagnetic properties. The electric and magnetic susceptibilities are different along with the director and perpendicular to the director. Upon application of an electric or magnetic field, the difference between the strength of dipole interaction parallel and perpendicular to the director generate a torque on the liquid crystalline media, which rotates the molecules and thus reorients the director. The sign of the anisotropy in the susceptibilities is responsible for the director orienting parallel or perpendicular to an applied field. The susceptibility anisotropy can be modified by the addition of permanent electric dipoles in the liquid crystal matrix, extending the capabilities of liquid crystals for applications where these susceptibilities are exploited, such as liquid crystal displays [2].

1.3 Enhancing Liquid Crystals: Carbon Nanotube Doping

Recently, liquid crystalline composites constructed by dispersion of various types of nanostructures have been studied extensively. Among these nanostructures, carbon nanotubes (CNTs) have received considerable attention due to their inherent, large anisotropy [3]–[5]. Carbon nanotubes are a subset of the fullerene family. They

are basically cylinders with a very high aspect ratio, over 1000. The length of the carbon nanotubes reaches the order of millimeters, but their diameters range in few nanometers. The CNTs can be thought of as a layer of graphene sheet rolled into the shape of a hollow cylinder. Carbon nanotubes were first discovered by Iijima in 1991 while producing fullerene (C60). The nanotubes that Iijima first produced were multi-walled carbon nanotubes (MWCNTs). Later, single-walled carbon nanotubes (SWCNTs) were also produced by Iijima and Ichihashi. Ever since these anisotropic nanostructures have been studied extensively due to their unique electrical, thermal and mechanical properties [6]. The shape anisotropy and resultant anisotropic properties of carbon nanotubes make them viable candidates for doping liquid crystals, themselves highly anisotropic materials. Several studies on such nanocomposites have been conducted, discussed in detail in the second chapter, and have yielded favourable, but varied, results that show dielectric enhancement, which directly affects the electro-optical properties of LC in general.

1.4 Aim of the Thesis

The thesis aims to present electro-optical studies conducted on carbon nanotube dispersed smectic 8CB nanocomposites and further reveal their effect on the elasticity and dielectric anisotropy of a smectic liquid crystal in its nematic phase. The dispersed MWCNTs are expected to enhance electro-optical properties, with higher susceptibility to the electric field and higher birefringence. The nanocomposites are formed by pristine and -COOH functionalized MWCNTs, each type being dispersed in two different concentrations by weight, 0.07 and 0.007 wt.%. The -COOH functionalization is meant to enhance the integration of MWCNTs into the liquid crystalline matrix. The study will present and discuss findings on these enhancements and if the intended effects have been realized by dispersing MWCNTs in LCs.

2. MATERIALS AND EXPERIMENTAL METHODS

In this chapter, the subject samples are introduced in detail, and measurement methods employed to examine their electro-optical properties are discussed.

2.1 Samples

The samples studied in the thesis are composed of one smectogen host, 8CB, and multi-walled carbon nanotubes, either with pristine or -COOH functionalized surfaces. The rationale for their selection, their relevant properties, and the method of composing them together to obtain the sample nanocomposites are discussed in the following subsections.

2.1.1 The host material: Octylcyanobiphenyl

8CB of 4-alkyl-4'-cyanobiphenyl (nCB) homologs was chosen as the nematic host for nanocomposites. Electro-optical properties of carbon nanotube dispersed smectogen nCB, with n = 8,9, have not been investigated as extensively as various nematic hosts, despite their photochemical stability and low ion concentration. In addition to this, they have low melting points and nematic - isotropic transition temperatures. These qualities make nCB smectogen suitable for commercial applications that involve in-plane switching and passive-matrix addressing display technologies [7]. However, dielectric and electro-optical characterization required for paving the way for such technologies have focused on nematic liquid crystal - carbon nanotube dispersions. 5CB (pentylcyanobiphenyl) [8,9], EBBA (4-ethoxybenzylidene-4'-n-butylaniline) [10], and nematic LC mixtures like E7 [11,12], MLC6601 [13], and 3017 [14] have been popular as host materials and shown to be enhanced by addition of carbon nanotubes. The number of studies with materials exhibiting both nematic and smectic A phases, such as 8CB, is scarcer. Examples of these studies include: a calorimetric study on transition temperatures of 8CB - carbon nanotube composite, which are

found to be lowered by 1.10 K [15]; an electrical conductivity study which revealed percolation behaviour in said composites [16]; a study on induced electroclinical effect in achiral smectogen host [17] and phase study of a negative dielectric anisotropy doped by CNT [18]. Despite the low number of studies, a variety of effects have been documented, which shows that smectogens are promising candidates as hosts for carbon nanotube composites.

The molecular structure of 8CB is given in Figure 2.1 [19]. While it is a rod-like molecule of 2 nm in length, the flexible alkyl chain gives the molecule more degrees of freedom than a pure nematic. The molecule is also polar, though the bulk is apolar, as liquid crystalline bulk tends to be [20]. The local polarity and Wan der Waals interactions with the flexible chains combine to create a more interactive host environment for dopants which, possibly, leads to a richer variety of enhancements to be observed in the resultant nanocomposite.

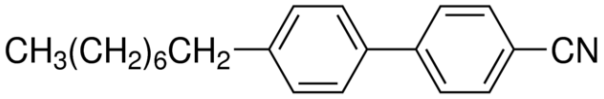

Figure 2.1 : Molecular structure of 8CB.

LC compound octylcyanobiphenyl (8CB), with purity better than 99.8 % as reported by the supplier, was purchased from AWAT Co. Ltd., Warsaw, Poland. No further purification was performed on the 8CB. The phase transition temperatures were reported to be TNI 0 = 40.5 C$^\circ$ for the nematic-isotropic (N–I) transition and TNA = 33.5 C$^\circ$ for the nematic-smectic A (N–SmA) transition.

2.1.2 Anisotropic dopant: Carbon nanotubes

Carbon nanotubes are single-atom-thick sheets of carbon, rolled into tubes of varying lengths. Depending on the process used to produce them, the nanotubes may either be single-walled, as formed from a single layer of rolled-up carbon, or multi-walled, formed by several concentric rolled up carbon sheets [6,21]. The anisotropic structure of carbon nanotubes enables their seamless incorporation into the liquid crystal host matrix and leads to the enhancement of viscoelastic [22], electrical [23,24], and electro-optical properties [23,25] and change phase transition characteristics of the

liquid crystal host [26]. While the potential of carbon nanotubes as liquid crystal dopants has been studied for some time now, these studies mostly involved nematic liquid crystals as hosts. These studies revealed the electro-optical and dielectric properties of nematic liquid crystals such as 5CB, EBBA and also some nematic LC mixtures after addition of carbon nanotubes. Studies on liquid crystal - carbon nanotube composites with both nematic and smectic A phases have been few in number, as mentioned above. However, these studies did not consider the effect of the functionalization of carbon nanotubes. The functionalization of carbon nanotubes may lead to better nanocomposites, as put forward in [24,27,28]. The carboxyl group (-COOH) functionalized carbon nanotubes have been shown to greatly enhance the dielectric permittivity of ferroelectric nematic liquid crystal while keeping the transition temperatures unchanged. The octadecylamine (ODA) functionalization of single-walled carbon nanotubes has also been shown to enhance electro-optic response and elastic constants of 8CB medium. Other than the enhancement of dielectric and electro-optical properties, with emphasis on liquid crystal applications, a more fundamental question has been raised by Sigdel and Iannacchione in their calorimetric investigation of the effect of CNTs on the nematic-isotropic (N-I) and the nematic-smectic A (N-SmA) transitions in 8CB - CNT nanocomposites [15]. The authors reported a downward shift in both transition temperatures, compared to pure 8CB, and thusly inferred that dispersion of CNTs in LC host causes the disorder. The calorimetric data, however, is not sufficient to conclude the disturbance of orientational order. More direct measurement of orientational order, such as birefringence, is required. So, while discovering the electro-optical characteristics of 8CB - MWCNT nanocomposites through optical measurements, it is possible to gain further insight into CNTs effect on the orientational order of a smectogen host.

Multiwalled Carbon Nanotubes, with diameters between 5 and 8 nm and lengths from 1 to 5 μm, were donated by Bayer, Germany. The -COOH functionalized MWCNTs has been donated by Prof. Dr. Ümit Tunca from ITU Chemistry Department.

2.1.3 Sample preparation

8CB liquid crystal - multi-walled carbon nanotube nanocomposites were prepared by the solvent dispersion method [21,23,43]. The MWCNT and 8CB, at desired weight fraction, are first added into high purity toluene (Carlo Erba). The weight fractions are calculated as

$$\phi = \frac{m_{CNT}}{m_{CNT} + m_{LC}} \tag{2.1}$$

The mixture is then heated to 43 °C, a temperature at which 8CB is isotropic liquid, and ultrasonicated for 5 hours at that temperature. The mixture is then subjected to constant magnetic stirring, and sonification at regular intervals to promote homogeneity, for 14 hours. During this time, toluene is evaporated. When the toluene is entirely evaporated from the mixture, the remaining mixture, still held at 43 C°, is introduced into ITO coated (< 30 Ω/sq) sandwich type planar LC cells (Instec Inc., USA) with a thickness 7.7 μm by capillary action. Two kinds of dopants are used: pristine and functionalized MWCNTs. Each type of dopant and 8CB was weighted on a sensitive scale (Sartorius SE Ultra-Micro Balance, 0.1 μg precision) to yield 0.007 and 0.07 weight fractions according to Eqn. 2.1. In total, four sample nanocomposites are obtained. A reference sample was also prepared with pure 8CB. Cells were hermetically sealed with epoxy once full.

The samples are required to retain the host's liquid crystalline phases and homogeneity in order to comply with the goals of this study, hence baseline checks are performed before any electro-optical measurements. The phase transition temperatures of nanocomposites were checked via differential scanning calorimetry (DSC) measurements (Perkin Elmer Pyris Diamond) by locating the maxima of the DSC peaks. The scanning rate of measurements was 5 K/min and the relevant datum were collected on a second cooling cycle [29]. Two peaks were observed in all samples in the relevant temperature range, belonging to nematic-isotropic and nematic-smectic A phase transitions. The DSC measurements are given in Figure 2.2. The phase structures of nanocomposites were also examined with a polarizing microscope. No phase separation nor agglomeration, both common problems with CNT dispersions,

was observed. The textures were homogeneous, which indicates an uniform director field, as seen in Figure 2.3. The cell spacing is known to filter out MWCNT aggregates larger than itself, letting in only aggregates too small to affect the director field [26,30].

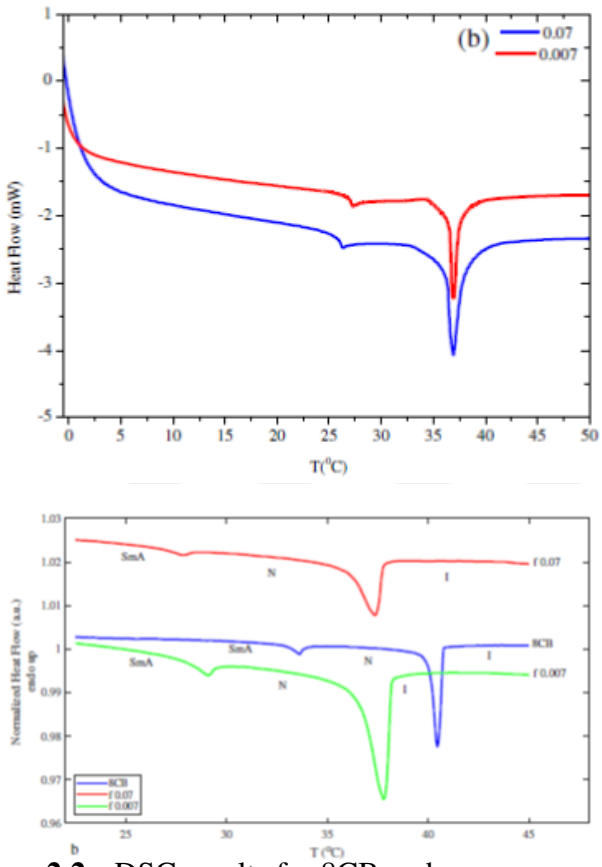

Figure 2.2 : DSC results for 8CB and nanocomposites.

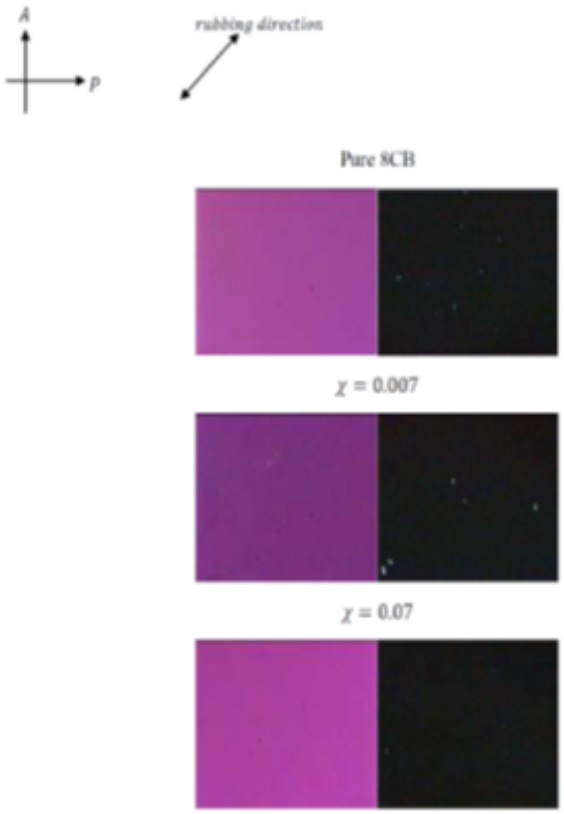

Figure 2.3 : Polarizing microscopy images of 8CB-MWCNT nanocomposites. The images are virtually same for both pristine and functionalized MWCNT dopants.

2.2 Experimental Methods

In this section, experiments used to study the electro-optical properties of nanocomposites are described in detail. Birefringence measurements are undertaken in order to study nematic and smectic A phases of nanocomposites through the nematic order parameter. With crossed polarizer measurements, the dependence of polarized light transmission through the samples with respect to temperature and the electric field strength is revealed. These measurements are followed by dielectric measurements, which yield a sensitivity of liquid crystalline medium to electric stimuli. The results are combined to profile the electro-optical characteristics of the nanocomposites.

2.2.1 Optical measurements

The nanocomposites were examined in two different optical setups: one which measures birefringence and one which only measures transmitted light intensity. Both birefringence and transmitted light intensity depend on the retardance across the

optical path through the sample. However, setups differ in the precision they offer. Birefringence measurements, as conducted here with a lock-in amplifier, yield much more precise figures and capture the changes in birefringence down to mK resolution in temperature, but they are slower and can not keep up with dynamic changes associated with electrical switching of liquid crystal. On the other hand, crossed polarizer light transmittance measurements are fast enough to track intensity changes during switching, they are less sensitive to temperature changes. Hence birefringence measurements are used to study liquid crystalline phases of nanocomposites and corroborate DSC and POM results, while electro-optical properties of the samples are investigated with light intensity measurements.

2.2.1.1 Light transmission measurement with crossed polarizors

One common method to study electro-optical properties of liquid crystalline samples is the crossed polarizer method. In a crossed polarizer setup, a coherent beam of light passes through one polarizer, a birefringent sample, rotated so that its optical axis is at 45° with respect to the first polarizer, and another polarizer after the sample, rotated 90° with respect to the first polarizer. The dependance of light intensity detected after the second polarizer, also called analyzer, on birefringence (Δn) of the sample is given by the equation

$$\Delta n = \frac{\lambda}{\pi d}[\sin^{-1}(I/I_0)] \tag{2.2}$$

where λ is the wavelength of the coherent light source, d is the thickness of the sample, I is the intensity of the light detected after the analyzer and I_0 is the initial intensity of the coherent beam. It should be noted here that, since birefringence is a sinusoidal function of light intensity, it is not possible to determine the birefringence of a sample at an arbitrary state with a single measurement. Measurements should start at a state where the birefringence of the sample is zero and continued until the desired state is reached by, for example, varying the sample temperature (starting at an isotropic state). Between the initial and final state, each extremum of the light intensity corresponds to

a $\pi/2$ increase in sample retardance, which is used to find the birefringence. The block diagram of the crossed polarizer setup is given in Figure 2.4.

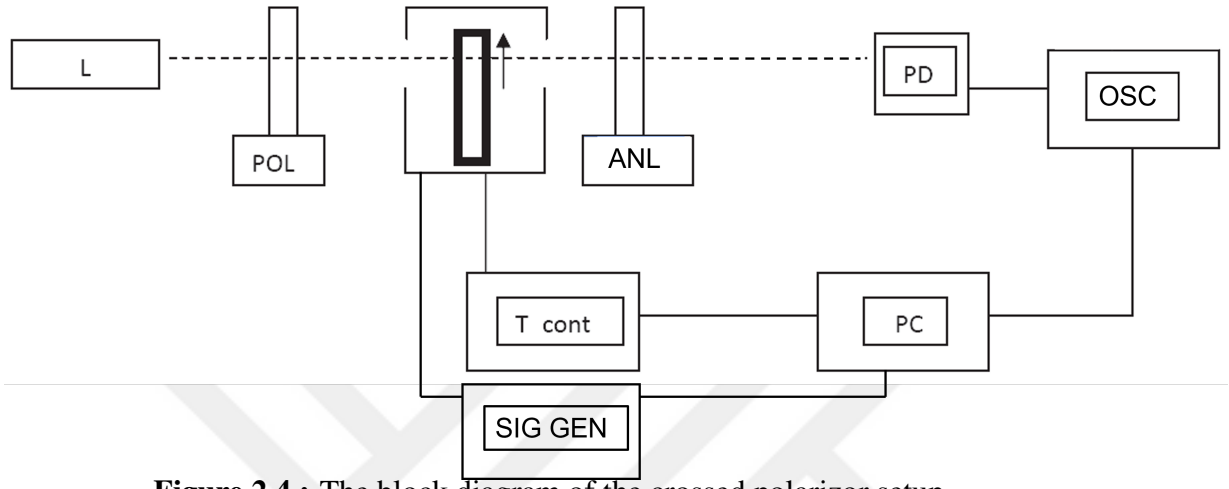

Figure 2.4 : The block diagram of the crossed polarizor setup.

In order to study the electro-optical properties, which, in the scope of this thesis, are threshold voltages and response times of Freédericksz transition, sample cells are connected to a signal generator. In addition to providing driving voltage for Freédericksz transitions at different temperatures, the signal generator also supplies a reference signal for the detection of light intensity signals via an oscilloscope. The driving signal is a 1 Hz square wave, which excites the sample cell for half a second and the sample shows relaxation behaviour in the other half. The driving signal is actually a 5 kHz square wave, modulated with a 1 Hz square wave envelope. A 5 kHz signal is applied in order to prevent surface polarization that occurs when a DC voltage is applied [31]. The reference signal is a 0.5 Hz square wave, which acts as the oscilloscope trigger, and makes it possible to capture the signal in the desired time frame. The switch between the capture of excitation or relaxation of the liquid crystalline sample is made by changing the phase of the driving signal with respect to the reference. The temperature of the sample is controlled down to ± 0.1 K, while measurements are performed. Also, in order to erase any residual effects from

switching, the samples are heated to the isotropic phase before being cooled down to the next temperature [8].

The signal generator used to drive the Freédericksz transitions in the sample cell is Rigol, Model DG1022. The waveforms generated by light intensity changes at the photodiode are captured by a Tektronix TDS210 digital oscilloscope. The temperature is controlled via Lakeshore 331, in a closed loop PID control scheme, with a PT-1000 sensor sourced from Omega Eng. Corp. The heater is a custom-made 50 Ω resistive element attached to a vertical sample holder. The polarizers and photodiode are sourced from Thorlabs Inc., while the 635 nm laser module is an OEM product. The data acquisition is coordinated by a LabVIEW program, with respect to sample temperature and driving voltage. The setup is covered with insulation to cut out light and air drafts in the laboratory, which is kept at 16 C° ±1 C° by climate control.

2.2.1.2 Birefringence measurements

Birefringence measurements of the samples were carried out with a rotating analyzer setup. The rotating analyzer method is a variation on crossed polarizers method, where the light intensity detected after the analyzer is dependent on the retardance of the birefringent sample. However, light intensity detection is noisy and prone to fluctuating signals. The rotating analyzer method gets around this issue by using modulated light intensity signal. The birefringent sample elliptically polarizes the incident modulated light. The ellipticity of the polarization here is directly proportional to the retardation of the sample, thus birefringence. A quarter-wave plate and a polarizer are placed successively after the sample and are both oriented at an angle of 45° to the optical axis of the sample. For a nematic liquid crystal sample under study, the selected optical axis would be the axis of planar orientation, where the long axii of the molecules lie. There is also a reference beam generated by another laser module which is modulated with the same angular frequency, incident on another photodiode. The elliptically polarized light leaving the sample is rendered plane-polarized, with a rotation of half the ellipticity angle. In this case, the modulated intensity signal is given by a term of an expansion as,

$$I(t) = I_0 \sin(2\omega t + 2\frac{\Delta n \pi d}{\lambda}) + ... \tag{2.3}$$

where λ is the wavelength of the coherent light source, d is the thickness of the sample, $I(t)$ is the intensity of the light detected after the analyzer, I_0 is the initial intensity of the coherent beam and ω is the modulating frequency. Since the AC signal generated by this modulated light can be captured very precisely by a lock-in amplifier, using the other modulated beam as the reference, the phase can be determined very accurately relative to the reference. The measured phase of the AC signal is directly proportional to the birefringence of the sample. The block diagram of the setup is given in Figure 2.5.

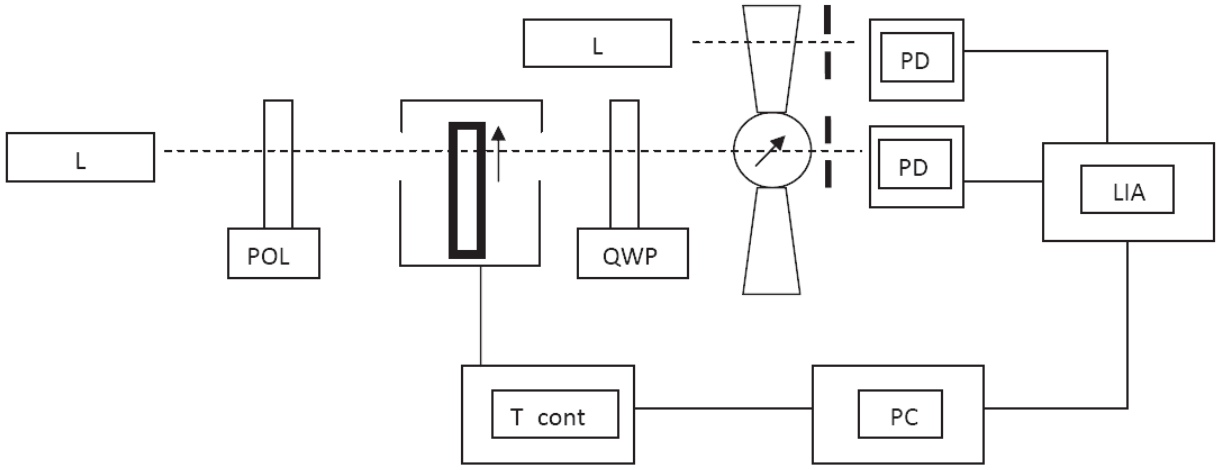

Figure 2.5 : The block diagram of the birefringence measurement setup.

The probing light is from a He-Ne laser, JDS Uniphase, at a wavelength of 633 nm. The polarizer, quarter-wave plate, rotating polaroid and photodiode are all sourced from Thorlabs Inc. . The phase measurements are made with a Stanford Research SR830 lock-in amplifier. The temperature of the sample is maintained by a custom-made 50 Ω resistive heater element placed directly on the opposite side of the sample cell holder and a PT-1000 temperature sensor, from Omega Eng. Corp., which is in direct contact with the sample cell, connected to a Lakeshore 335 temperature controller, in a closed-loop PID control. The sample holder is thermally cut off from the room by a 2 cm thick metal cover with a large thermal mass. The whole setup is also covered and insulated from air drafts in the laboratory, which is also kept at 16 °C ±1 °C by climate control. The data is collected by a LabVIEW program.

2.2.2 Dielectric measurements

The electro-optical properties of liquid crystals depend largely on their dielectric anisotropy, as it is the dielectric anisotropy that determines the susceptibility of the medium to an applied electrical field. The dielectric anisotropy is the difference between dielectric constants parallel and perpendicular to the long axis of the molecules, which constitutes the nematic director in bulk. In this study, these dielectric constants are determined in two different alignment modes: planar and homeotropic. In order to determine the dielectric constant in a particular alignment, the capacitance of the sample cell is measured in that alignment mode, so that electric field is either parallel or perpendicular to the long axii of the aligned molecules. The alignment of liquid crystalline material inside the sample cell is decided by the surface interaction between the liquid crystal and the inner cell wall. The schematic of alignments inside the planar and homeotropic sample cells are given in Figure 2.6.

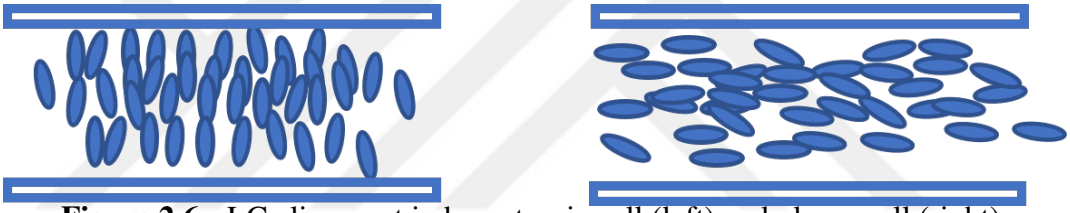

Figure 2.6 : LC alignment in hometropic cell (left) and planar cell (right).

The dielectric constant is extracted from the measured capacitance by

$$\Delta\varepsilon(T) = \frac{C_{LC}(T)}{C_{empty}(T)} \tag{2.4}$$

where $C_{LC}(T)$ is the capacitance of the filled sample cell and $C_{empty}(T)$ is the capacitance of the empty sample cell at a certain temperature. By measuring the capacitance of the empty cell for all relevant temperatures, one can eliminate the temperature-dependent effects on measured capacitance such as expansion and contraction of the sample cell dividers, and isolate the temperature-dependent behaviour of dielectric constants.

The capacitance of the samples is measured with a 10 kHz 0.3 V_{rms} probing signal, using a GW-Instek Model 8110-G precision LCR meter with a capacitance range

of 0.01 pF to 1 F. The 10 kHz probing frequency is chosen to be out of the dielectric relaxation region of the host liquid crystal [32]. At 10 kHz, MWCNTs do not show exhibit dipole orientation or space charge dynamics, thus asymmetric distribution of MWCNTs through the host is also avoided [26]. The homeotropic alignment is achieved by commercially available, 9 μm thick, ITO-coated (10 Ω/sq) homeotropic cells, sourced from AWAT Co. Ltd., Warsaw, Poland. The dielectric constants parallel to the nematic director are measured in the same sample cells used in electro-optical measurements, sourced from Instec Inc., USA. The capacitance vs. temperature datum is collected during cooling cycles, during which stability of liquid-crystalline alignment is expected to be better than those in heating cycles. The same heater, temperature sensor, control scheme, and insulation are used as in electro-optic measurements.

3. 8CB DOPED WITH MULTI-WALLED CARBON NANOTUBES

In this chapter, the results of the experiments conducted on 8CB - MWCNT nanocomposites are given. The chapter is divided into four sections. The first section contains the precise birefringence measurements to in order ascertain nematic ranges and order. The second section presents dielectric measurements to study the variations in dielectric anisotropy - temperature dependence with respect to dopant concentration. The third section discusses electro-optical measurements, which include response times and threshold voltages. In the fourth and final section, the viscoelastic properties of the bulks are obtained from dielectric and electro-optical measurements. The results shared within this chapter are meant to convey the changes to bulk optical anisotropy, elastic energy, and susceptibility to electrical field

3.1 Birefringence Measurements

The birefringence Δn of 8CB doped with carbon nanotubes is measured in the temperature region between 24° C to 45° C. The birefringence vs. temperature data are presented with a temperature shift with respect to nematic to the isotropic transition temperature. Birefringence is measured to be zero in the isotropic phase of all 8CB-MWCNT nanocomposites, no sign of a pre-transitional effect in isotropic phases has been measured. Therefore, nematic to isotropic transition temperature T_{IN} is chosen to be the lowest temperature at which birefringence is zero. The nematic to smectic A transition temperatures are decided from the discontinuity in the second derivative of the birefringence data with respect to the temperature around the N - Sm A transition. The difference between two transition temperatures gives the width of the stable nematic temperature region. In Table 3.1, the transition temperatures and nematic region widths (NR) are given.

The birefringence vs. temperature data with shifted temperatures are given in Figure 3.1. Compared to pure 8CB, only 0.07 wt.% nanocomposite shows enhanced Δn; Δn

Table 3.1 : N-I and SmA-N transition temperatures of pure 8CB and nanocomposites with nonfunctionalized MWCNTs.

Sample	T_{NI} (° C)	T_{NA} (° C)	NR (K)
8CB	40.5	33.5	7
0.007 %wt.	37.10	26.96	10.14
0.07 %wt.	36.50	26.90	9.6

is both higher in the nematic phase, as well as in the smectic A phase. The 0.007 wt.% nanocomposite is less birefringent in the whole nematic range, while its birefringence values in the smectic A phase are similar to that of pure 8CB. Right below the T_{NI}, after the transition into the nematic state, Δn shows weakly first-order characteristics, increasing sharply with decreasing temperature. As the nematic molecular order increases in lower temperatures, Δn gradually increases. The rate at which Δn of the nanocomposites increases as the temperature drops is similar to each other and to the pure 8CB in the nematic region, although pure 8CB exhibits a slightly faster rate.

The smectic order arising in the nematic phase is known to be detectable by observing the enhancement of Δn, which signals the increase in the order of the long molecular axis [1,33]. The increased nematic order is associated with the onset of smectic layering [34]. This increase is reflected in the change in the first derivative of Δn with respect to temperature as the temperature nears N-SmA transition [33]. It is with this change in derivative that one can infer the transition temperature T_{NA}. It is also worth noting that the enhancement of birefringence by N-SmA transition is depressed in both nanocomposites in comparison to pristine 8CB.

Table 3.2 : N-I and SmA-N transition temperatures of pure 8CB and nanocomposites with nonfunctionalized MWCNTs.

Sample	T_{NI} (° C)	T_{NA} (° C)	NR (K)
8CB	40.5	33.5	7
0.007 %wt.	37.17	26.96	10.21
0.07 %wt.	36.95	26.37	10.58

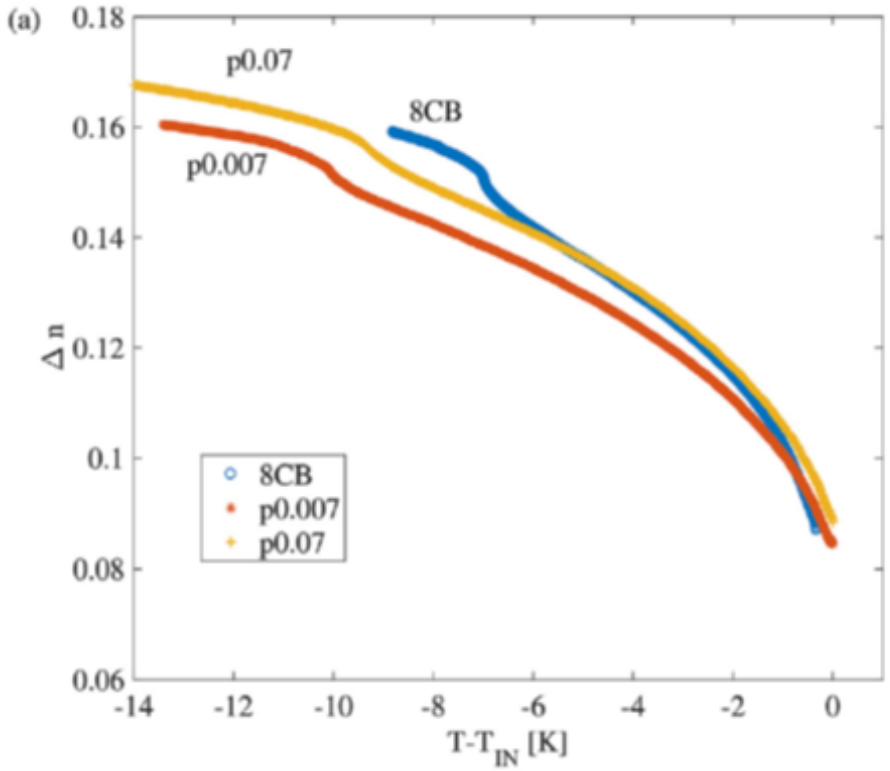

Figure 3.1 : Birefringence vs. temperature over the nematic and smectic A phases of pure 8CB and nanocomposites with nonfunctionalized MWCNTs.

3.2 Dielectric Measurements

The dielectric measurements are conducted in the nematic and smectic regions of the samples, between temperatures 24° C to 45° C. The dielectric anisotropy vs. temperature datum are presented in separate Figures 3.2, 3.3 and 3.4, without any temperature shifts. The transition temperatures extracted from the extrema in the first derivative of the datum are presented in Table 3.2. As seen in those extracted from birefringence vs. temperature datum, T_{NI} and T_{NA} are both lowered by 3.7 K and 5.2 K in nanocomposites, which extends the nematic region by 3 K, in comparison to pure 8CB.

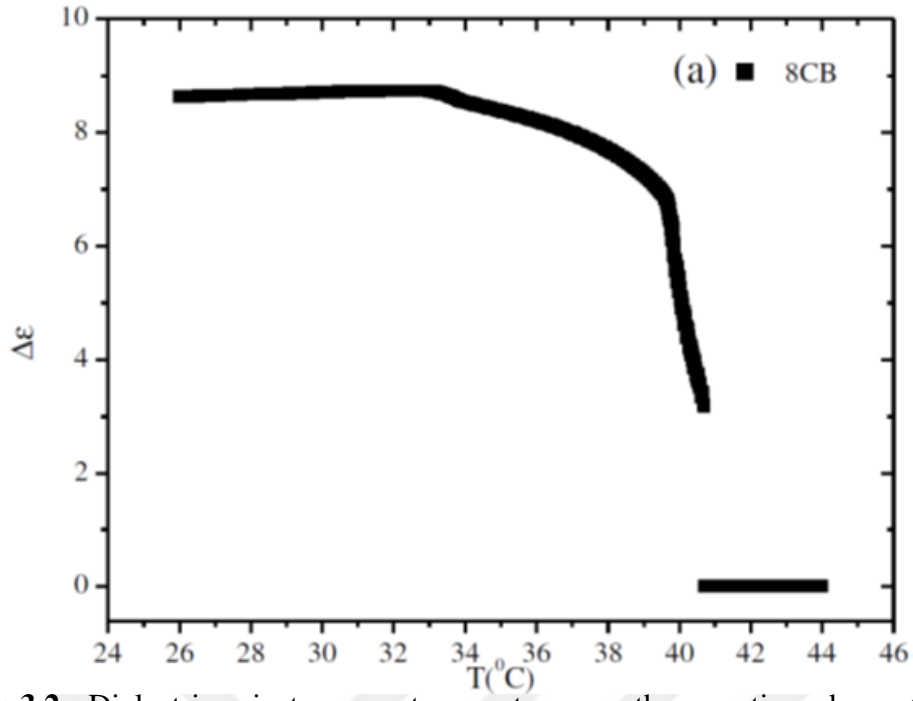

Figure 3.2 : Dielectric anisotropy vs. temperature over the nematic and smectic A phases of pure 8CB.

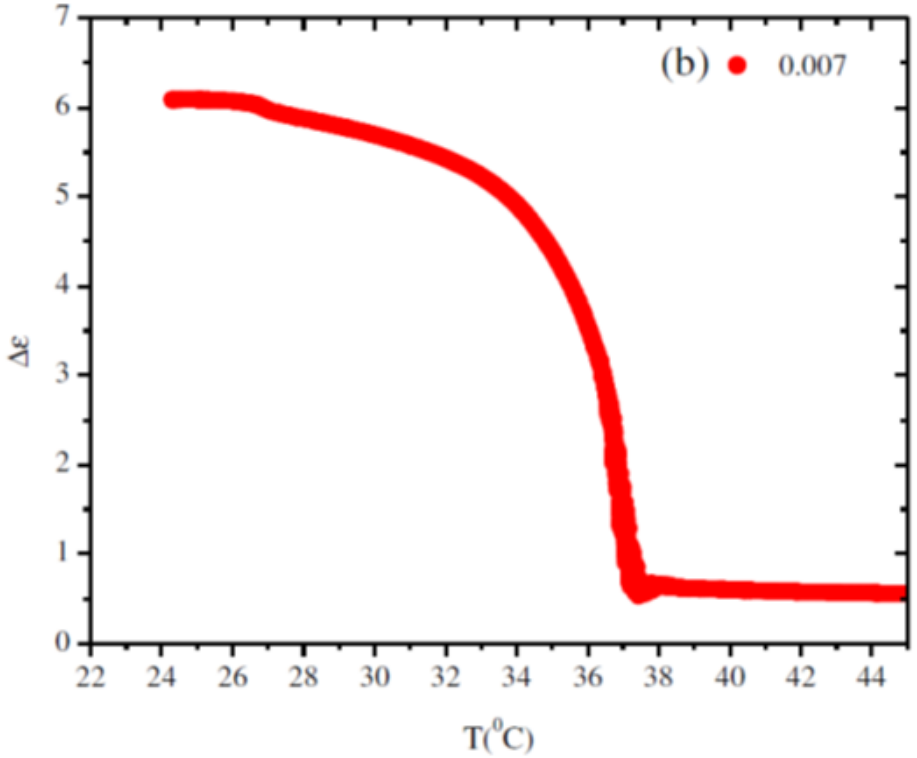

Figure 3.3 : Dielectric anisotropy vs. temperature over the nematic and smectic A phases of 0.007 wt.% MWCNT nanocomposite.

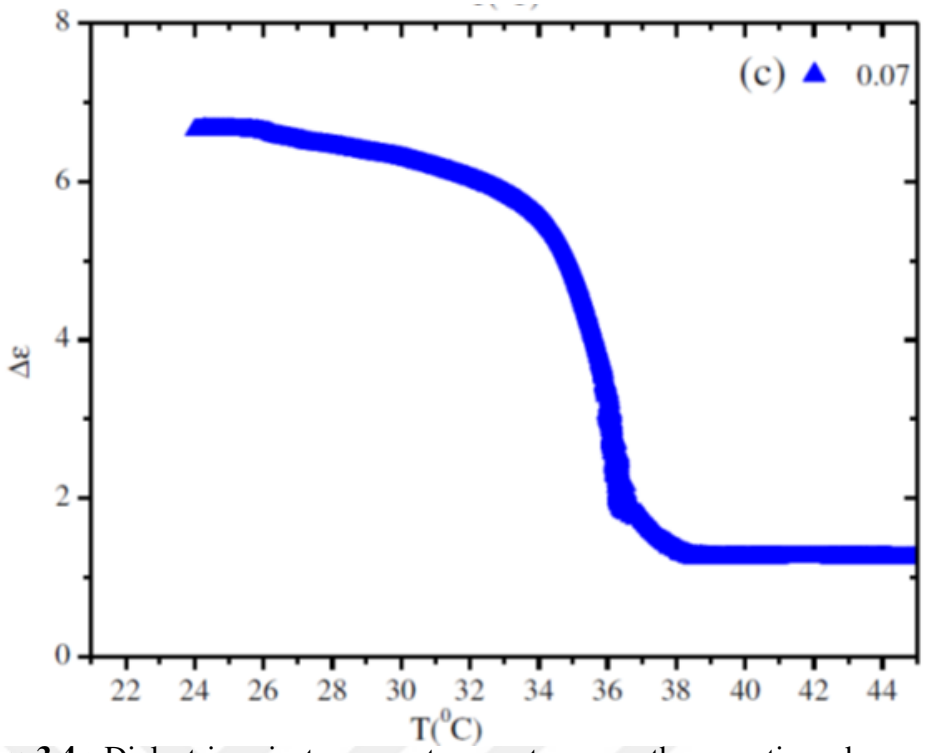

Figure 3.4 : Dielectric anisotropy vs. temperature over the nematic and smectic A phases of 0.07 wt.% MWCNT nanocomposite.

The pure 8CB has zero $\Delta\varepsilon$ in the isotropic phase, with a sharp jump to non-zero values at its isotropic to the nematic transition temperature. The zero $\Delta\varepsilon$ in the isotropic phase of 8CB indicates the absence of pre-transitional effects in pure 8CB. The coupling between the liquid crystal molecules and the surfaces of dispersed MWCNTs is known to induce local orientational order around the MWCNTs, which accounts for the non-zero dielectric anisotropy in doped samples [26,35]–[37]. The value of $\Delta\varepsilon$ in the isotropic phase for 0.07 wt.% nanocomposite is higher than 0.007 wt.% one. The isotropic to nematic transition itself is also affected, the sharp jump at 8CB is replaced by a slope beginning about 2 K above the transition temperatures. While the slope is evident in 0.007 wt.% nanocomposite, it is much more pronounced in the 0.07 wt.% one.

As the temperature is lowered further gradual increase of dielectric anisotropy is observed in all samples, mirroring the increase in orientational order as shown by birefringence measurements. Upon approaching T_{NA}, the onset of short-range smectic ordering further enhances the order. Similar behaviour has been reported by Das Gupta et al. before [38]. However, unlike birefringence, dielectric anisotropy decreases when

the temperature is further lowered in the smectic A phase. This decrease is attributed to the anti-parallel correlation between dipoles, the neighbor polar molecules of 8CB whose aromatic cores overlap [39]–[41]. In contrast to pure 8CB, both nanocomposites exhibit increasing dielectric anisotropy with decreasing temperature in their smectic phases.

The sample with the highest dielectric anisotropy overall in the region of interest is the pure 8CB. 0.07 wt.% nanocomposite follows, with a drop in dielectric anisotropy around 1.5 in the smectic range, and 0.007 wt.% nanocomposite has the lowest dielectric anisotropy, about 2 lower than the pure 8CB in the smectic region. Another point of interest is the variation of the behaviours of $\Delta\varepsilon$ in the nematic region: While pure 8CB mimics its own birefringence vs. temperature, tied to the variation of nematic order parameter S, nanocomposites have a less steep increase of $\Delta\varepsilon$ following the N-I transition.

3.3 Electro-optical Measurements

The intensity of transmitted light through sample cells in a crossed polarizers setup is measured as a function of applied voltage in the temperature interval covering nematic and smectic A phases.

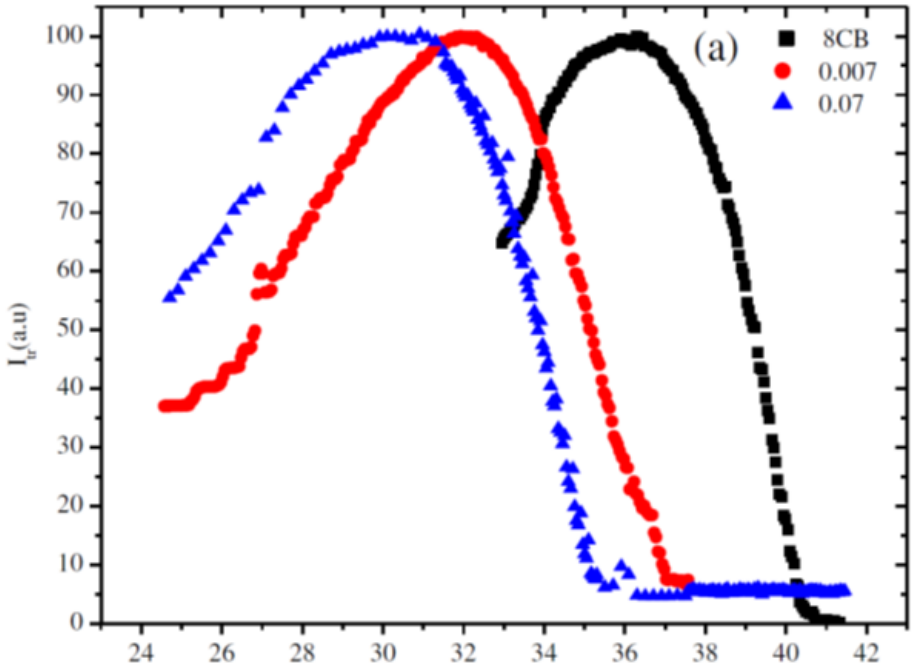

Figure 3.5 : Transmitted light intensity vs. temperature curves of all samples over the nematic and smectic A phases.

In Figure 3.5 the transmitted intensity, I_{tr}, is given as a function of temperature. For pure 8CB liquid crystal, the nematic to isotropic transition temperature is the temperature at above which electric field-induced switching does not occur. The transition temperatures decided for the samples by this criteria are 40.5°C for pure 8CB, 37°C for 0.007 wt.%, and 36°C for 0.07 wt.% respectively. In the nanocomposites, there are non-zero values of transmitted light intensity due to weak residual nematic order, called pseudo-nematic domains [26,36,42]. Thus, the transition temperature T_{NI} of nanocomposites is determined from the extrema of the first derivative of I_{tr}(T) with respect to temperature T. These transition temperatures are in accordance with the temperatures where distinct Freédericksz threshold voltages vanish [1,8]. While the pseudo-nematic domains are electrical field responsive, the isotropic phase offers no restoring force, which explains the lack of distinct threshold voltages [42]. As the temperature is lowered, light transmission increases in all samples as a result of increasing nematic order. The intensity drop that occurs when samples are cooled further is also due to increasing order, but in this case, increasing nematic order further increases the retardance to a point where transmitted light intensity decreases because of the phase difference between extraordinary and ordinary components of the polarized light.

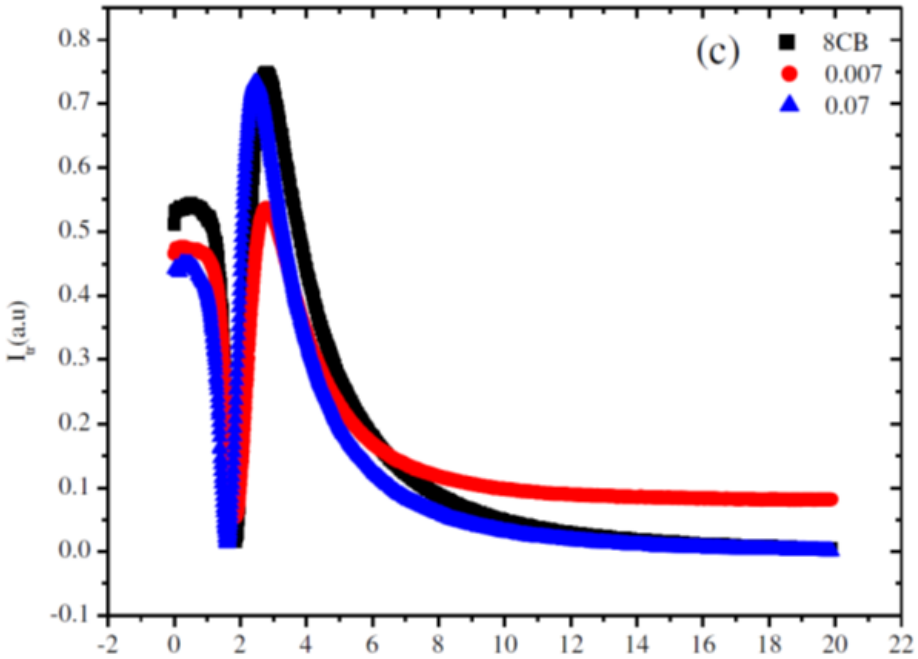

Figure 3.6 : Transmitted light intensity vs. voltage at shifted temperature $T - T_{NI} = -2.6K$ for all samples.

Transmitted intensity I_{tr} variations of 8CB and MWCNT nanocomposites, with respect to the applied voltage, are given in Figure 3.6, at shifted temperature $T - T_{NI} = -2.6K$ in the nematic region. As the applied voltage is increased, Freédericksz transition between planar and homeotropic anchoring occurs in all samples. The extrema, peaks, and valleys, that occur in the transmitted light intensity as the voltage is increased are due to the phase difference between ordinary and extraordinary waves in liquid crystalline media. This phase difference is brought on by the reorientation of the director. The bulk with positive dielectric constant transitions from planar to homeotropic alignment, where molecules are in line with the electrical field lines. The saturation at higher voltages suggests that the reorientation of surface fractions due to external field in all studied samples [2,10,16,31,43]. Also, there were no time-dependent changes in voltage applied state or voltage removed state. The field-dependent transitions were all reversible at all temperatures studied, without any memory effects that were observed in negative dielectric constant liquid crystals [10,16,43]. The hysteresis is also absent from both pure and doped samples. The doping that produced nanocomposites did not change the shape of I_{tr} curve obtained from the pure 8CB.

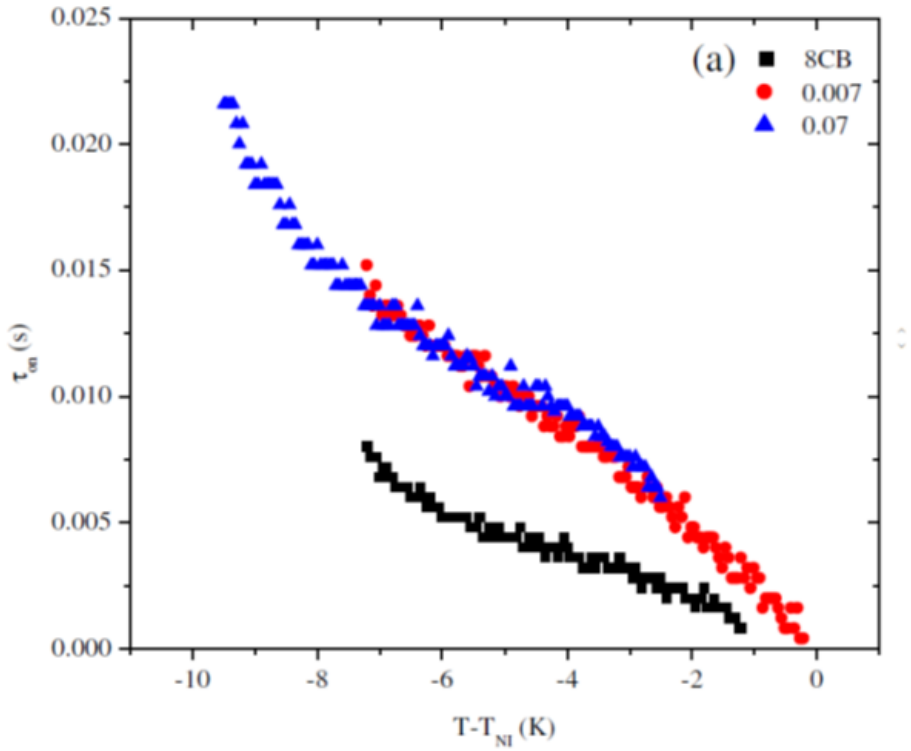

Figure 3.7 : Voltage-on response times vs. shifted temperature at 10 V switching voltage for 8CB and nonfunctionlized MWCNT nanocomposites.

The characteristic time parameters voltage-on and voltage-off response times are measured with respect to temperature and applied voltage. The measurement of response times is carried out by recording the light transmission during the application and removal of the electrical field generated by a voltage above the threshold at a constant temperature. The voltage-on response time, t_{on}, is the time required to reach the homeotropic state [44] after the voltage is applied to the sample. The voltage-off response time is the time that the director takes to relax to its former planar state after the removal of the voltage at a constant temperature. In Figure 3.7, voltage-on times for all samples with respect to shifted temperature $T - T_{NI}$ at 10 V switching voltage are given. It is evident that voltage-on times are increased with dopants, although the amount at which it increased is measured to be close for both nanocomposites between -2 K and -7 K shifted temperatures. The voltage-on response t_{on} decreases with increasing temperature.

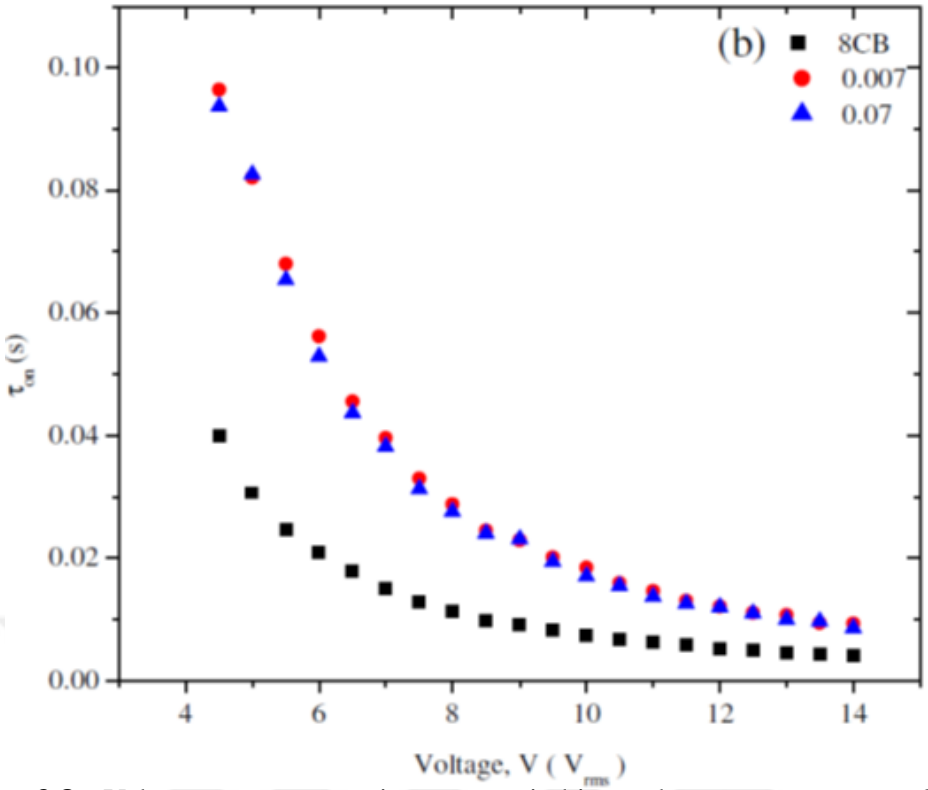

Figure 3.8 : Voltage-on response times vs. switching voltage at $T - T_{NI} = -2K$ for 8CB and nonfunctionlized MWCNT nanocomposites.

In Figure 3.8, the voltage-on response time vs. switching voltage at $T - T_{NI} = -2$ K is given. The nanocomposites t_{on} values are again close, as with the vs. temperature data. The response times decrease by increasing the switching voltage. While the behaviour of 8CB and nanocomposites are similar, the nanocomposites react to electrical fields at lower voltages much slower. The difference of t_{on} of pure 8CB and nanocomposites at 5 V is 45 ms, while at 14 V it is 5 ms.

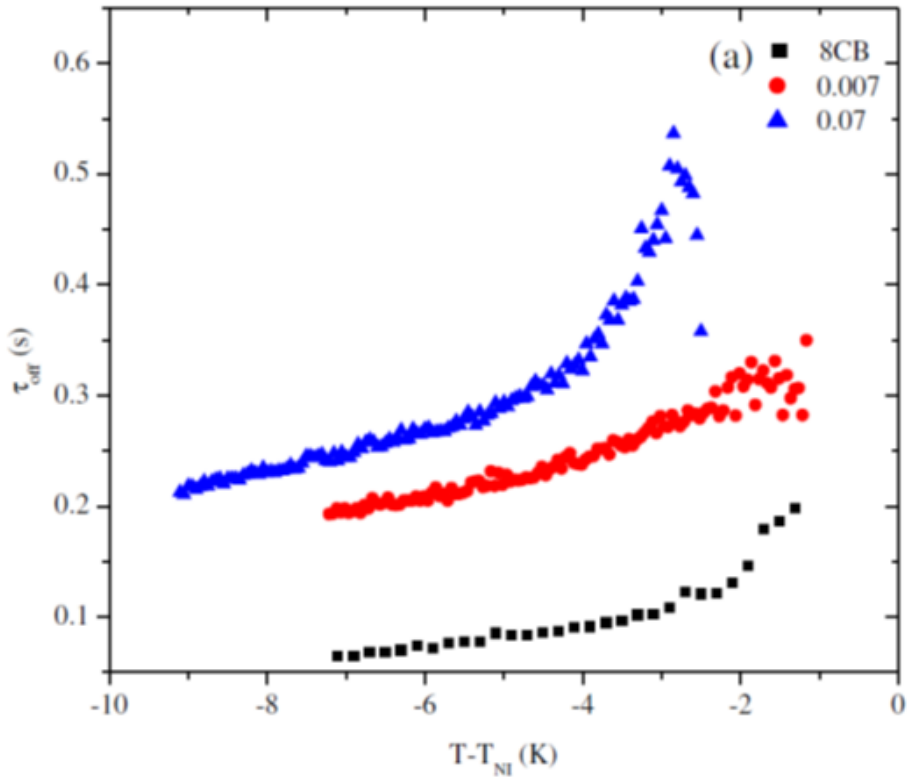

Figure 3.9 : Voltage-off response times vs. shifted temperature for 8CB and nonfunctionlized MWCNT nanocomposites.

The relaxation times, also called voltage-off response times, with respect to temperature are given in Figure 3.9. While pure 8CB has the fastest relaxation, unlike the t_{on} data, voltage-off response times are distinguishable between nanocomposites: 0.007 wt.% is faster than the 0.07 wt.%. Below -3 K shifted temperature, voltage-off response times of pure 8CB and 0.007 wt.% drop linearly with temperature. A similar behaviour is present for 0.07 wt.% below -5 K.

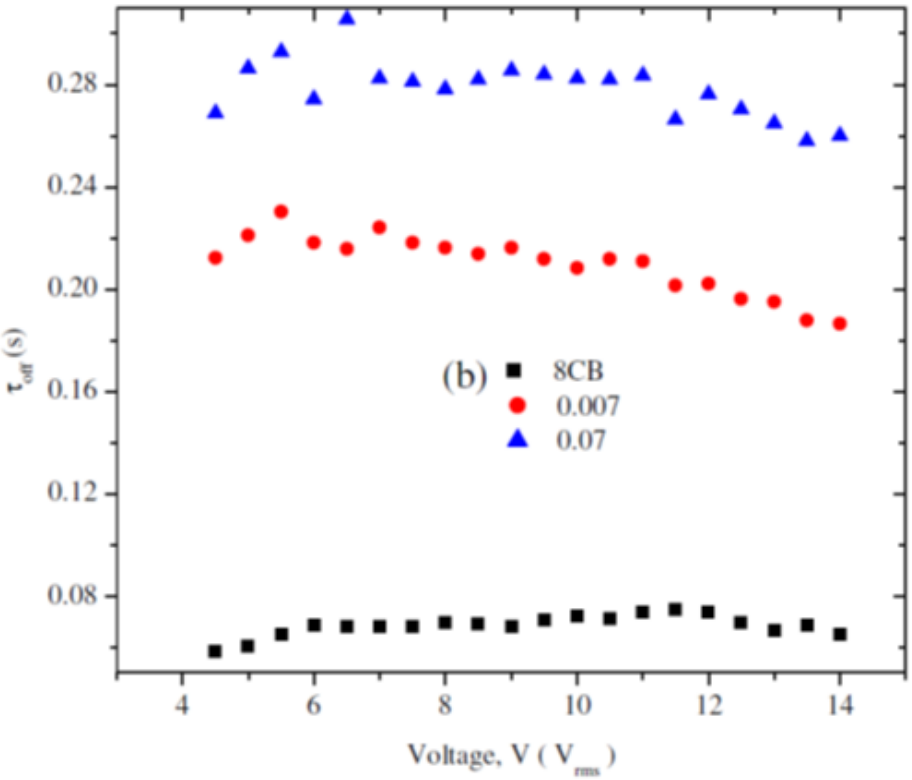

Figure 3.10 : Voltage-off response times vs. shifted temperature for 8CB and nonfunctionlized MWCNT nanocomposites.

The voltage-off response times of all samples with respect to applied voltage is given in Figure 3.10. The variations for applied, and then removed, voltages are inside a 50 ms band for all samples in the studied voltage interval, and tend to decrease as the voltage increases with nanocomposites. However, the variations are more likely to be artefacts of light intensity measurements as the contrast between states changes with applied voltage and measurement of response times depend on the percentages of that light intensity difference.

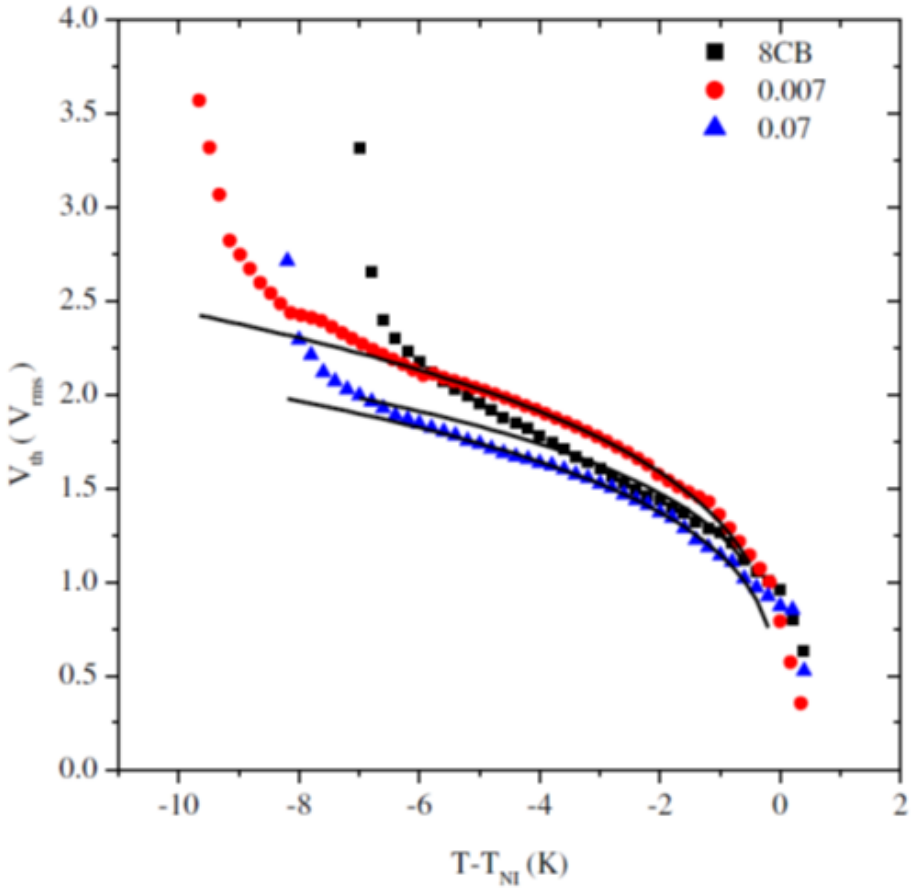

Figure 3.11 : Threshold voltages vs. shifted temperature for 8CB and nonfunctionlized MWCNT nanocomposites.

Threshold voltages in the temperature region of interest are extracted from I_{tr} vs. voltage data. The threshold voltage V_{th} vs. shifted temperature data for all samples is presented in Figure 3.11. The threshold voltage is defined to be the voltage at which average birefringence of the liquid crystalline sample begins to vary with the application of said voltage [2,44]. The threshold voltages of 0.07 wt.% nanocomposite are lower than pure 8CB, while for 0.007 wt.% one they are higher in most of the nematic region. The threshold voltage values are close at the beginning of the nematic phase and increase with decreasing temperature. As the smectic phase is approached, V_{th} of all samples increase sharply, which coincides with the onset of smectic layering.

3.4 Splay Constants And Rotational Viscosities

By using the dielectric constant, threshold voltage, voltage-off response time datum visco-elastic properties of 8CB and nanocomposites are ascertained. Two temperature dependent properties are calculated: splay elastic constant and rotational viscosity.

Splay elastic constants K_{11} are calculated by using the dielectric and V_{th} datum in the following relation [2,45]:

$$K_{11} = \varepsilon_0 \Delta\varepsilon (\frac{V_{th}}{\pi})^2 \tag{3.1}$$

where ε_0 is the permittivity of free space. As seen in Figure 3.12, the splay elastic constant of pure 8CB is highest in the whole nematic region. The 0.007 wt.% follows, with a slightly flatter increase with decreasing temperature and 0.07 wt.% nanocomposite is the last with least increase in K_{11} as smectic phase is approached. Therefore, by increasing MWCNT concentration, splay elastic constant of the bulk is lowered.

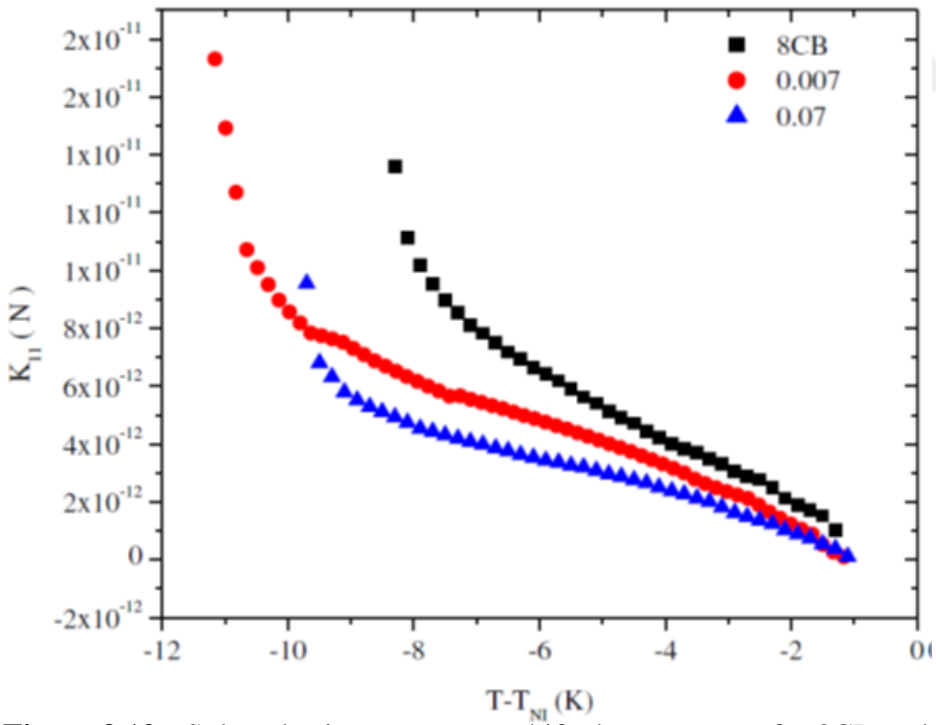

Figure 3.12 : Splay elastic constant vs. shifted temperature for 8CB and nonfunctionlized MWCNT nanocomposites.

The temperature dependence of the rotational viscosity γ in the nematic phase is obtained for all samples under study of using the relation [46,47]:

$$\gamma = t_{off} K_{11} (\frac{\pi}{d})^2 \tag{3.2}$$

where d is the thickness of the sample cell. The γ vs. shifted temperature data for all samples is presented in Figure 3.13. Pure 8CB has the lowest rotational viscosity. Both nanocomposites have significantly higher values, with 0.07 wt.% nanocomposite having slightly higher rotational viscosity than the 0.007 wt.% nanocomposite. The rotational viscosities for all samples increase with decreasing temperature, although rate of increase is higher in 0.007 wt.% nanocomposite. In contrast to K_{11}, rotational viscosity increases with increasing concentration of MWCNTs.

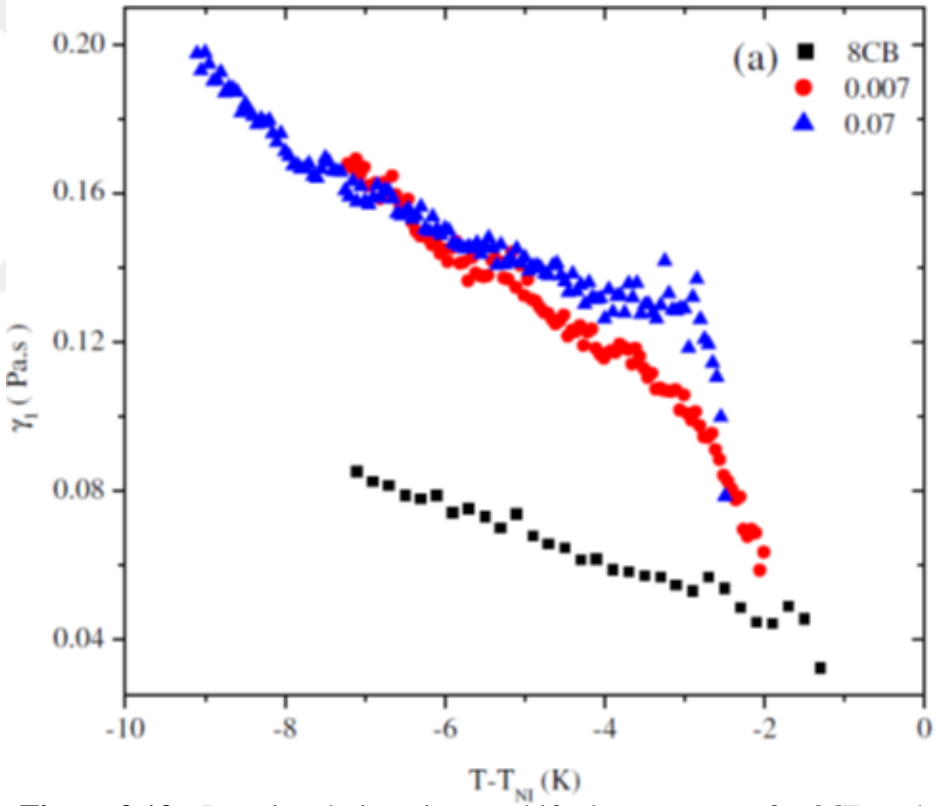

Figure 3.13 : Rotational viscosity vs. shifted temperature for 8CB and nonfunctionlized MWCNT nanocomposites.

4. 8CB DOPED WITH -COOH TREATED CARBON NANOTUBES

In this chapter, the results of the experiments conducted on 8CB - COOH functionalized MWCNT nanocomposites are presented. The chapter is composed of four sections. In the first section, the precise birefrigence measurements, which show the nematic ranges and order, are given. The second section presents dielectric measurements, where the dielectric anisotropy - temperature dependence for all samples are discussed. In the third section response time and threshold voltage measurements are presented. The fourth and final section contains the viscoelastic properties of the bulks that are derived from dielectric and electro-optical measurements. The changes to bulk optical anisotropy, elastic energy and susceptibility to electrical field that are caused by COOH functionalized MWCNTs are investigated in this chapter.

4.1 Birefringence Measurements

The birefringence Δn of 8CB doped with COOH functionalized multi-walled carbon nanotubes are measured in the temperature region between 24° C to 45° C. The COOH functionalized MWCNTs are called "fMWCNT" from here on. The birefringence vs. temperature data are presented with a temperature shift with respect to nematic to the isotropic transition temperature. Birefringence is measured to be zero in the isotropic phase of all 8CB-fMWCNT nanocomposites, no sign of a pre-transitional effect in isotropic phases has been measured. Therefore, nematic to isotropic transition temperature T_{IN} is chosen to be the lowest temperature at which birefringence is zero. The nematic to smectic A transition temperatures are decided from the discontinuity in the second derivative of the birefringence data with respect to the temperature around the N - Sm A transition. The difference between two transition temperatures gives the width of the stable nematic temperature region. In Table 4.1, the transition temperatures and nematic region widths (NR) are given.

Table 4.1 : N-I and SmA-N transition temperatures of pure 8CB and nanocomposites with functionalized MWCNTs.

Sample	T_{NI} (° C)	T_{NA} (° C)	NR (K)
8CB	40.41	33.56	6.85
0.007 %wt.	37.54	29.44	8.1
0.07 %wt.	38.56	30.19	8.37

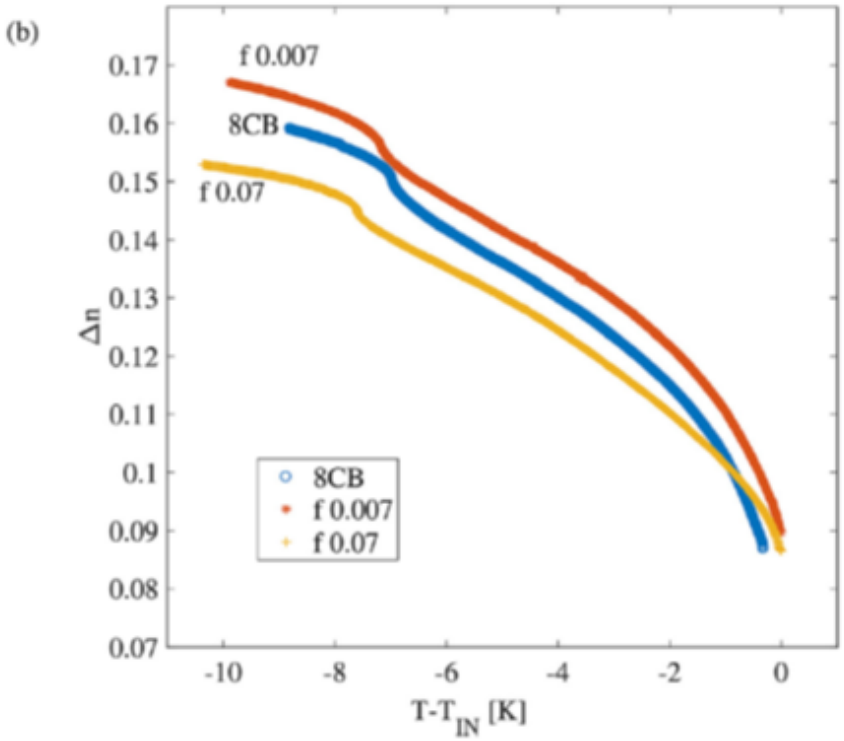

Figure 4.1 : Birefringence vs. temperature over the nematic and smectic A phases of pure 8CB and nanocomposites with functionalized MWCNTs.

The birefringence vs. temperature data with shifted temperatures are given in Figure 4.1. Compared to pure 8CB, only f0.007 wt.% nanocomposite shows enhanced Δn; Δn is both higher in the nematic phase, as well as in the smectic A phase. The 0.07 wt.% nanocomposite is less birefringent in the whole nematic range, while its birefringence values in the smectic A phase are similar to that of pure 8CB. Right below the T_{NI}, after the transition into the nematic state, Δn shows weakly first order characteristics, increasing sharply with decreasing temperature. As the nematic molecular order increases in lower temperatures, Δn gradually increases. The rate at which Δn of the nanocomposites increases as the temperature drops are similar to each other and to the pure 8CB in the nematic region, although pure 8CB exhibits a slightly faster rate. It is

noteworthy that the f0.07 wt.% exchanged places with 0.007 wt.% (non-functionalized MWCNT) and f 0.007 wt.% with 0.07 wt.% in their placement.

The smectic order arising in the nematic phase is known to be detectable by observing the enhancement of Δn, which signals the increase in order of the long molecular axis [1,33]. The increased nematic order is associated with onset of smectic layering [34]. This increase is reflected in the change in the first derivative of Δn with respect to temperature as the temperature nears N-SmA transition [33]. It is with this change in derivative that one can infer the transition temperature T_NA. It is also worth noting that the enhancement of birefringence by N-SmA transition is depressed, like with the non-functionalized MWCNTs, in both nanocomposites in comparison to pristine 8CB.

4.2 Dielectric Measurements

The dielectric measurements are conducted in the nematic and smectic region of the samples, between temperatures 24° C to 45° C. The dielectric anisotropy vs. temperature datum are presented in Figure 4.2 with $T - T_{NI}$ temperature shift.

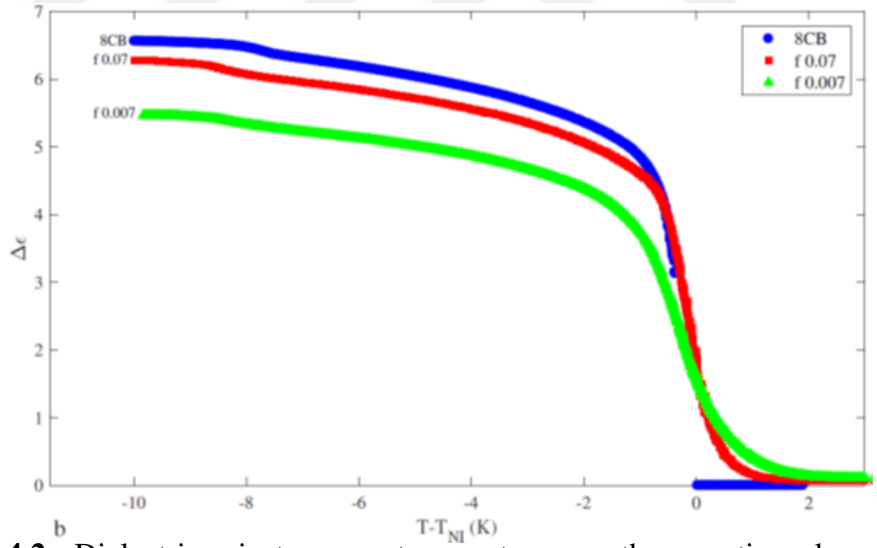

Figure 4.2 : Dielectric anisotropy vs. temperature over the nematic and smectic A phases of pure 8CB and nanocomposites with functionalized MWCNTs.

The pure 8CB has zero $\Delta\varepsilon$ in the isotropic phase, with a sharp jump to non-zero values at its isotropic to the nematic transition temperature. The zero $\Delta\varepsilon$ in the isotropic phase of 8CB indicates the absence of pre-transitional effects in pure 8CB. The coupling between the liquid crystal molecules and the surfaces of dispersed fMWCNTs, like

non-functionalized MWCNTs, induces local orientational order around the MWCNTs, which accounts for the non-zero dielectric anisotropy in doped samples [26,35]–[37]. The value of $\Delta\varepsilon$ in isotropic phase for f0.007 wt.% nanocomposite is higher than f0.07 wt.% one, once again exchanging places from non-functionalized MWCNT datum. The isotropic to nematic transition itself is again affected, the sharp jump at 8CB is replaced by a slope beginning about 2 K above the transition temperatures. The slope is much more pronounced in the f0.007 wt.% nanocomposite compared to 0.07 wt.% one, in contrast to results from non-functionalized MWCNTs.

As the temperature is lowered further gradual increase of dielectric anisotropy is observed in all samples, mirroring the increase in orientational order as shown by birefringence measurements. Upon approaching T_{NA}, the onset of short range smectic ordering further enhances the order. Similar behaviour has been reported by Das Gupta et al. before [38]. However, unlike birefringence, dielectric anisotropy decreases when the temperature is further lowered in the smectic A phase. This decrease is attributed to the anti-parallel correlation between dipoles, the neighbour polar molecules of 8CB whose aromatic cores overlap [39]–[41]. In contrast to pure 8CB, both nanocomposites exhibit increasing dielectric anisotropy with decreasing temperature in their smectic phases, like their non-functionalized counterparts.

The sample with the highest dielectric anisotropy over all in the region of interest is the pure 8CB. f0.07 wt.% nanocomposite follows, with only a drop in dielectric anisotropy around 0.2 in the smectic range, and f0.007 wt.% nanocomposite has the lowest dielectric anisotropy, about 1 lower than the pure 8CB in the smectic region. Another point of interest is the variation of the behaviours of $\Delta\varepsilon$ in the nematic region: While pure 8CB mimics its own birefringence vs. temperature, tied to the variation of nematic order parameter S, nanocomposites have less steep increase of $\Delta\varepsilon$ following the N-I transition. The dielectric anisotropies are higher in fMWCNT nanocomposites than pristine MWCNT ones.

4.3 Electro-optical Measurements

Intensity of tranmitted light through sample cells in a crossed polarizers setup is measured as a function of applied voltage in the temperature interval covering nematic and smectic A phases.

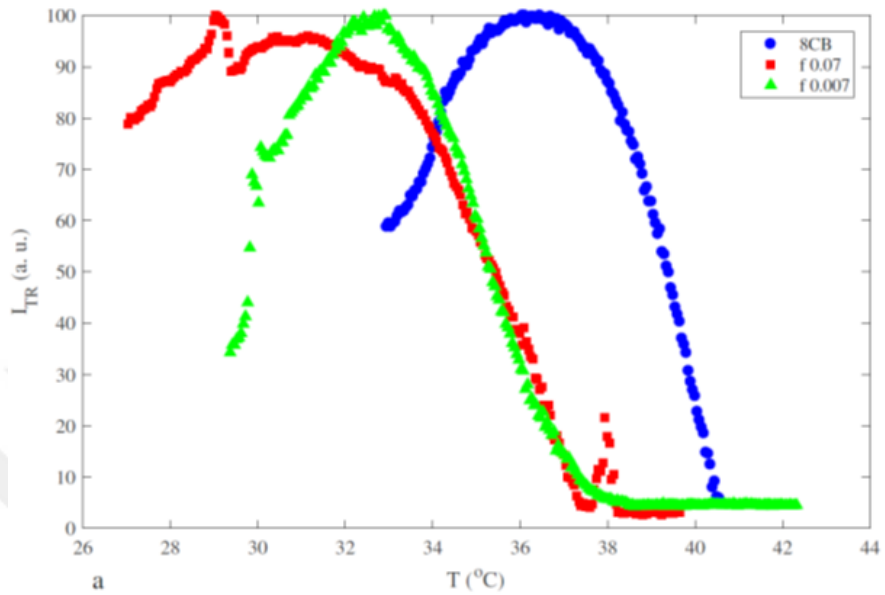

Figure 4.3 : Transmitted light intensity vs. temperature curves of all samples over the nematic and smectic A phases.

In Figure 4.3 the transmitted intensity, I_{tr}, is given as a function of temperature. For pure 8CB liquid crystal, the nematic to isotropic transition temperature is the temperature at above which electric field induced switching does not occur. The transition temperatures decided for the samples by this criteria are 40.5°C for pure 8CB, 38.2°C for f0.007 wt.% and 37.2°C for f0.07 wt.% respectively. In the nanocomposites, there are non-zero values of transmitted light intensity due to weak residual nematic order, so called pseudo-nematic domains [26,36,42]. Thus, the transition temperature T_{NI} of nanocomposites is determined from the extrema of the first derivative of I_{tr}(T) with respect to temperature T. These transition temperatures are in accordance with the temperatures where distinct Freédericksz threshold voltages vanish [1,8]. While the pseudo-nematic domains are electrical field responsive, the isotropic phase offers no restoring force, which explains the lack of distinct threshold voltages [42]. As the temperature is lowered, light transmission increases in all samples as a result of increasing nematic order. The intensity drop that occurs when

samples are cooled further is also due to increasing order, but in this case, increasing nematic order further increases the retardance to a point where transmitted light intensity decreases because of the phase difference between extraordinary and ordinary components of the polarized light wave.

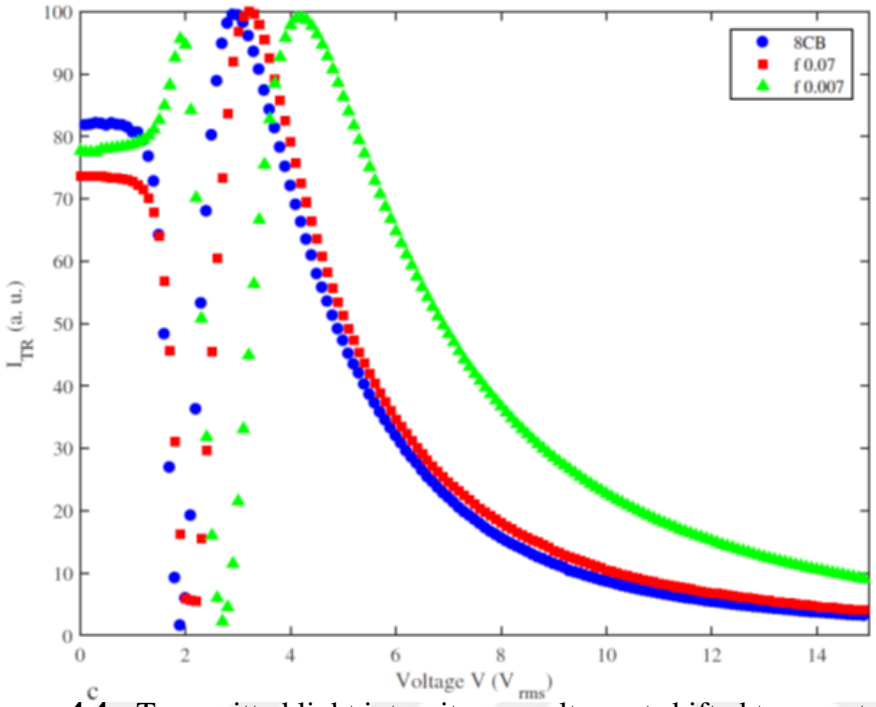

Figure 4.4 : Transmitted light intensity vs. voltage at shifted temperature $T - T_{NI} = -2.6K$ for all samples.

Transmitted intensity I_{tr} variations of 8CB and fMWCNT nanocomposites, with respect to the applied voltage, are given in the Figure 4.4, at shifted temperature $T - T_{NI} = -2.6K$ in the nematic region. As the applied voltage is increased, Freédericksz transition between planar and homeotropic anchoring occurs in all samples. The extrema, peaks and valleys, that occur in the transmitted light intensity as the voltage is increased are due to the phase difference between ordinary and extraordinary waves in liquid crystalline media. This phase difference is brought on by the reorientation of the director. The bulk with positive dielectric constant transitions from planar to homeotropic alignment, where molecules are in line with the electrical field lines. The saturation at higher voltages suggests that the reorientation of surface fractions due to the external field in all studied samples [2,10,16,31,43]. Also there were no time dependent changes in voltage applied state or voltage removed state. The field dependent transitions were all reversible at all temperatures studied, without

any memory effects that were observed in negative dielectric constant liquid crystals [10,16,43]. The hysteresis is also absent from both pure and doped samples. The doping that produced nanocomposites did not change the shape of I_{tr} curve obtained from the pure 8CB.

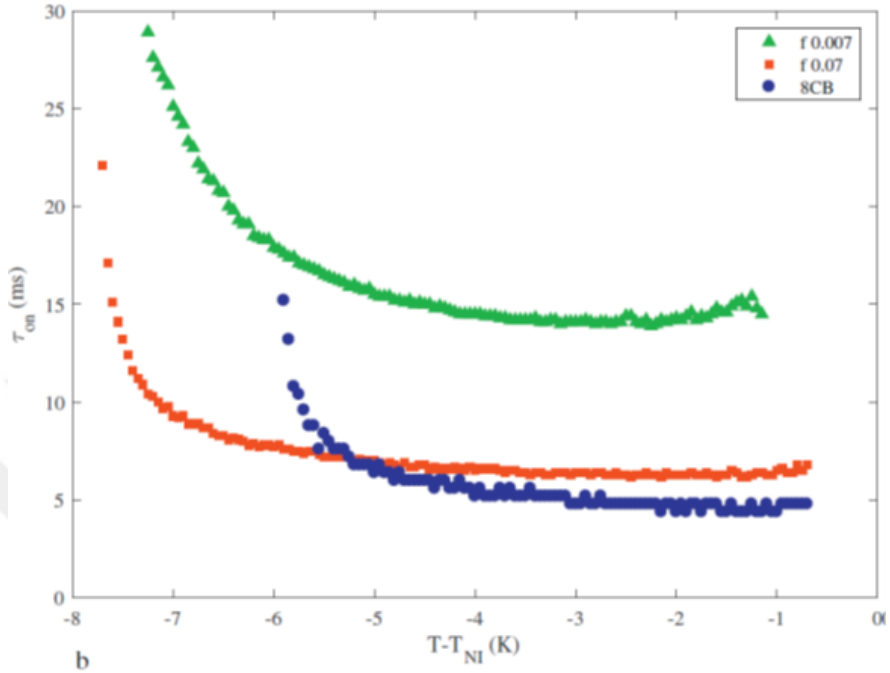

Figure 4.5 : Voltage-on response times vs. shifted temperature at 10 V switching voltage for 8CB and functionlized MWCNT nanocomposites.

The characteristic time parameters voltage-on and voltage-off response times are measured with respect to temperature and applied voltage. The measurement of response times is carried out by recording the light transmission during the application and removal of the electrical field generated by a voltage above the threshold at a constant temperature. The voltage-on response time, t_{on}, is the time required to reach the homeotropic state [44] after the voltage is applied to sample. The voltage-off response time is the time that the director takes to relax to its former planar state after the removal of the voltage at constant temperature. In Figure 4.5, voltage-on times for all samples with respect to shifted temperature $T - T_{NI}$ at 10 V switching voltage are given. The voltage-on times of fMWCNT doped nanocomposites are increased, but f0.07 wt.% voltage-on response times are very close to pure 8CB's response times compared to f0.007 wt.%, despite the higher concentration of fMWCNT. The

voltage-on response t_{on} decreases with increasing temperature for all samples, with divergent behaviour when nearing the SmA phase.

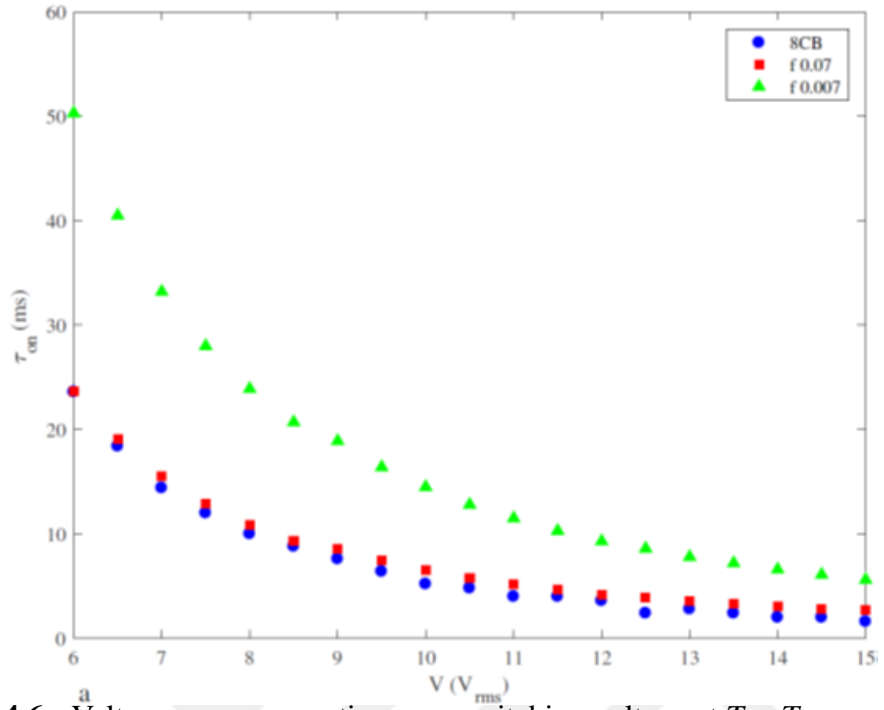

Figure 4.6 : Voltage-on response times vs. switching voltage at $T - T_{NI} = -2K$ for 8CB and functionlized MWCNT nanocomposites.

In Figure 4.6, the voltage-on response time vs. switching voltage at $T - T_{NI} = -2$ K is given. The pure 8CB and f0.07 wt.% nanocomposite t_{on} values are again close. The response times decrease by increasing the switching voltage. While the behaviour of 8CB and nanocomposites are similar, the f0.007 wt.% nanocomposite react to electrical fields at lower voltages much slower. The difference of t_{on} of pure 8CB and f0.007 wt.% nanocomposite at 6 V is 26 ms, while at 14 V it is 4 ms.

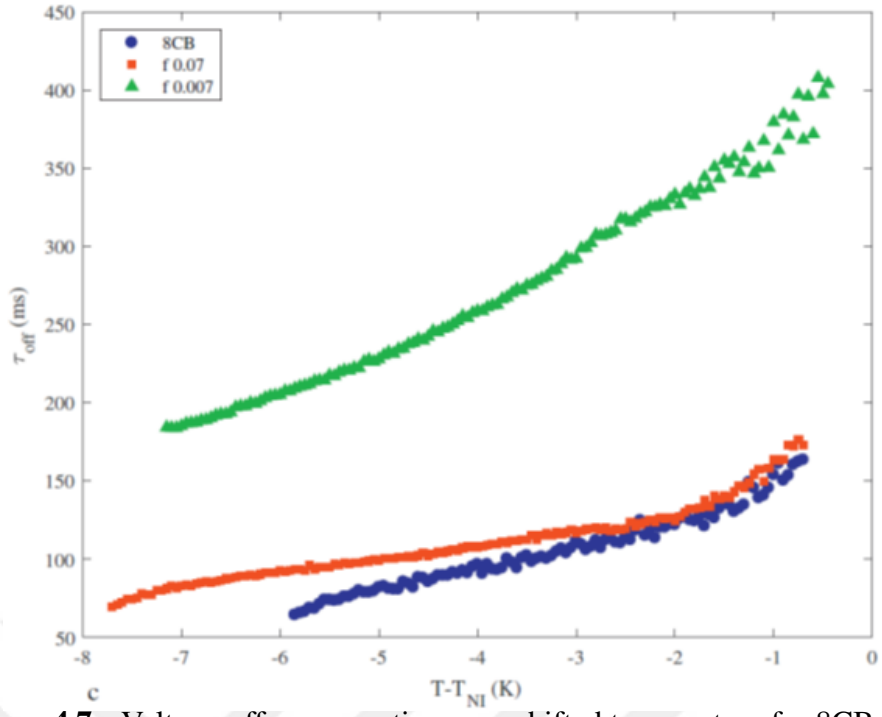

Figure 4.7 : Voltage-off response times vs. shifted temperature for 8CB and functionlized MWCNT nanocomposites.

The voltage-off response times (relaxation times) with respect to temperature are given in Figure 4.8. The pure 8CB has the fastest relaxation, as it did with the non-functionalized nanocomposites. Voltage-off response times of pure 8CB and f0.07 wt.% nanocomposite are close. The f0.007 wt.% nanocomposite is much slower than both of them. Below -3 K shifted temperature, voltage-off response times of pure 8CB and f0.07 wt.% drop almost linearly with temperature. A similar behaviour is present for f0.007 wt.% below -4 K.

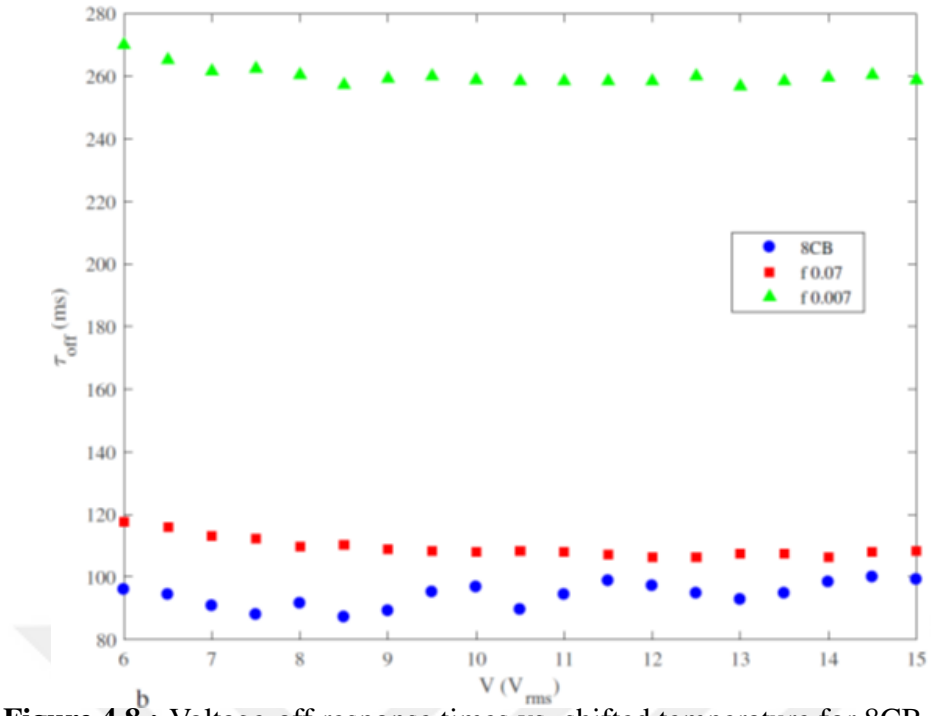

Figure 4.8 : Voltage-off response times vs. shifted temperature for 8CB and functionalized MWCNT nanocomposites.

The voltage-off response times of all samples with respect to applied voltage is given in Figure 4.8. The variations with respect to applied, and then removed, voltages are inside a 20 ms for all samples in the studied voltage interval, and tend to decrease as the voltage is increased with nanocomposites. As with the pristine MWCNT data set, the variations are more likely to be artefacts of light intensity measurements as the contrast between states changes with applied voltage and measurement of response times depend on the percentages of that light intensity difference.

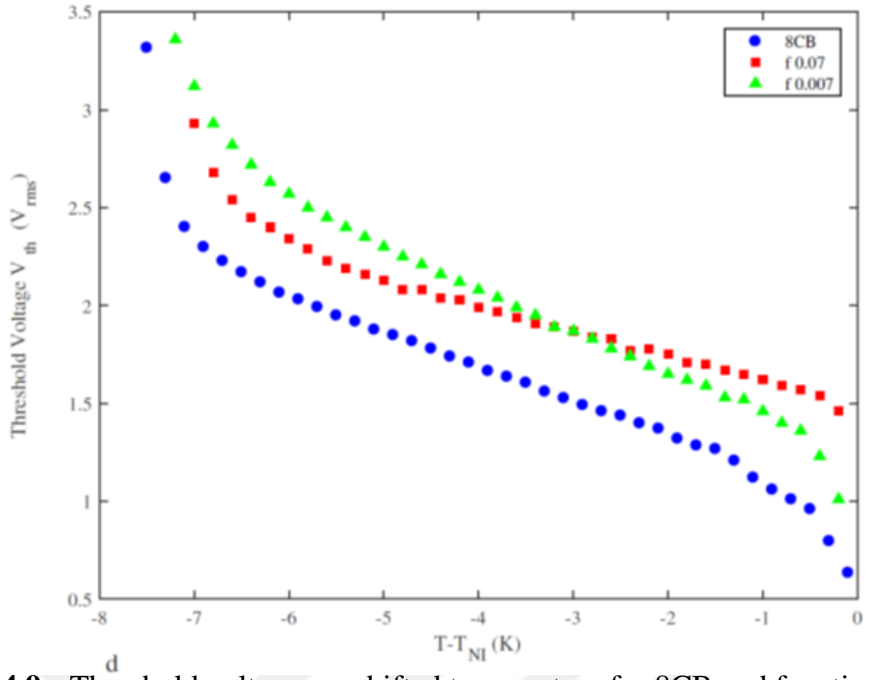

Figure 4.9 : Threshold voltage vs. shifted temperature for 8CB and functionalized MWCNT nanocomposites.

Threshold voltages in the temperature region of interest are extracted from I_{tr} vs. voltage data. The threshold voltage V_{th} vs. shifted temperature data for all samples is presented in Figure 4.9. The threshold voltage is defined to be the voltage at which average birefringence of the liquid crystalline sample begins to vary with the application of said voltage [2,44]. The threshold voltages of both nanocomposites are higher than pure 8CB. While V_{th} of 8CB and f0.007 wt.% increase with a similar slope as the temperature drops, but f0.07 wt.% is dissimilar: Its threshold voltages are higher than the other two above -3 K shifted temperature and in between the two below that point. As the temperature nears the nematic-smectic A transition temperature, V_{th} of all samples increase sharply, which coincides with the onset of smectic layering.

4.4 Splay Constants And Rotational Viscosities

By using the dielectric constant, threshold voltage, voltage-off response time datum visco-elastic properties of 8CB and nanocomposites are ascertained. Two temperature dependent properties are calculated: splay elastic constant and rotational viscosity.

Splay elastic constants K_{11} are calculated by using the dielectric and V_{th} datum in the following relation [2,45]:

$$K_{11} = e_0 \Delta e (\frac{V_{th}}{\pi})^2 \tag{4.1}$$

where e_0 is the permittivity of free space. As seen in Figure 4.10, the splay elastic constants of samples are very close, with pure 8CB having the lowest value compared to functionalized MWCNT nanocomposites. The f0.007 wt.% is in-between the other two for most of the nematic phase. The form of the K_{11} as a function of temperature is very similar in all samples, with only a slight increase with increased concentration. However, it must be noticed the differences between K_11 values of the samples, though small, are more pronounced closer to nematic - isotropic transition point, while as the temperature drops and smectic A phase is approached, splay constant values grow closer.

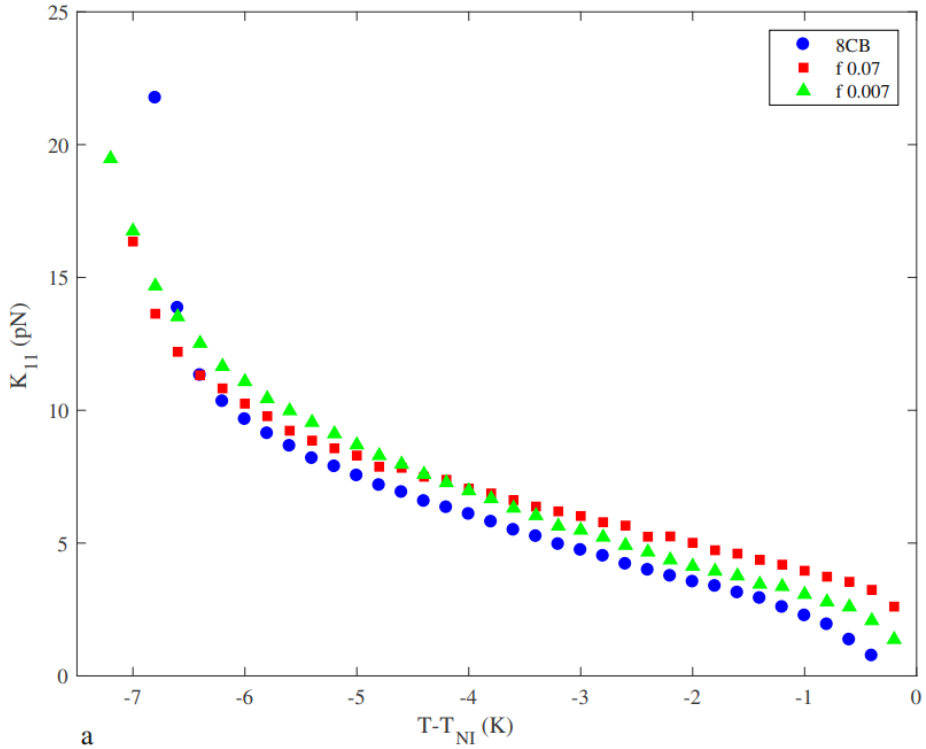

a

Figure 4.10 : Dielectric anisotropy vs. temperature over the nematic and smectic A phases of 0.07 wt.% MWCNT nanocomposite.

The temperature dependence of the rotational viscosity γ in the nematic phase is obtained for all samples under study of using the relation [46,47]:

$$\gamma = t_{off} K_{11} (\frac{\pi}{d})^2 \tag{4.2}$$

where d is the thickness of the sample cell. The γ vs. shifted temperature data for all samples is presented in Figure 4.11. Pure 8CB has the lowest rotational viscosity. f0.07 wt.% nanocomposite has slightly higher values than 8CB in the nematic region. f0.007 wt.% places significantly above the other two. The rotational viscosities for all samples increase with decreasing temperature. It is worth underlining that the lower concentration functionalized MWCNT nanocomposite f0.007 wt.% has the highest rotational viscosity, which is in contrast with the results obtained from nanocomposites with untreated MWCNTs. Also, the rotational viscosities of f0.007 wt.% is significantly higher than 8CB, non-functionalized MWCNT nanocomposites and f0.07 wt.% nanocomposite.

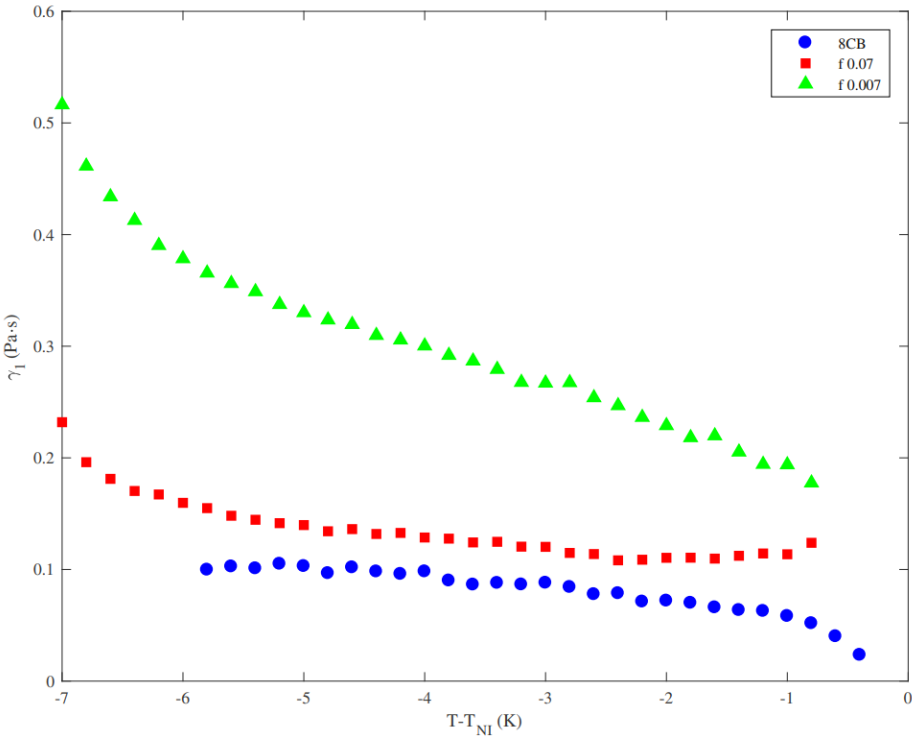

Figure 4.11 : Rotational viscosity vs. shifted temperature for 8CB and functionalized MWCNT nanocomposites.

5. CONCLUSIONS

5.1 Shifts In Transition Temperatures And Order Parameters

The overall trend for MWCNT, functionalized and non-functionalized, dispersed smectic liquid crystal nanocomposites' transition temperatures are downwards. Similar downshifts in transition temperatures have been reported for 8CB-MWCNT [43] and 5CB-SWCNT [48] dispersions, for 8CB dispersed with gold and silver nanoparticles [49]. The downward shift in T_{NI} and T_{NA} is evidence of disordering effects brought on by dilution [26,49]. However, the amount of transition temperature shift and the resultant nematic range differs between types of dispersed MWCNT. While pristine MWCNTs caused 42 % of the increase in the nematic range compared to pure 8CB, functionalized MWCNTs only caused 8.6 % increase. It should be noted that the size of T_{NI} and T_{NA} downward shifts follow the amount of dispersed MWCNTs with the pristine MWCNT nanocomposites, however the inverse is true for COOH functionalized MWCNT nanocomposites. The effect of MWCNT dispersion on phase order is better grasped through the investigation of birefringence datum. The lower concentration of pristine MWCNTs lowered the birefringence, but higher concentration one has very close birefringence to pure 8CB, in the nematic range, if only slightly higher closer to T_{NI}. Closer to nematic to smectic A transition, the birefringence values follow the order of T_{NA} transition temperatures. With COOH functionalized MWCNT dispersions, order samples have higher T_{NA} and vice versa. But with COOH functionalized MWCNTs, the order of T_{NA}s, and thus birefringences, is different: f0.007 wt.% has higher birefringence overall, while the birefringence of f0.07 wt. % nanocomposite is lowered. It was asserted that a strong anchoring due to $\pi - \pi$ electron stacking between 5CB-MWCNT molecules would enhance the nematic order parameter [44], and it appears this holds true for lower concentrations of functionalized MWCNTs, but fails on higher concentrations and non-functionalized MWCNTs. It is noteworthy that the nematic range extension and the downward shift

of transition temperatures are lower with functionalized MWCNTs, which means the dilution effect is smaller and they are better incorporated into the LC matrix. However, better incorporation is not enough to enhance the order, which is suggested by the lower birefringence of f0.07 wt.%. The fact that the birefringence enhancement is only observed in the lowest concentration dispersion with surface functionalization suggests that for any order enhancement to occur MWCNTs must seamlessly be incorporated into nematic liquid crystal matrix through LC-MWCNT interactions while MWCNTs remain sparse enough through the matrix so they do not interact with each other through elastic medium.

5.2 The Affect On Electro-Optical Parameters

5.2.1 Dielectric anisotropies, threshold voltages

Dielectric anisotropies of all studied nanocomposites are reduced, compared to pure 8CB. It is remarkable that despite the birefringence increase in one nanocomposite, f0.007 wt.%, the dielectric anisotropy of that nanocomposite is also decreased. f0.007 wt.% has lower dielectric anisotropy than 0.007 wt. its non-functionalized counterpart, despite the connection between anisotropic properties and order parameter. Charge redistribution due to dispersion of MWCNTs are likely to be effective. This, in effect, should increase threshold voltages, as the nanocomposites are less susceptible to the electric field. Indeed, the threshold voltages for 0.007 wt.%, f0.07 wt.%, f0.007 wt.% samples are increased. The threshold voltages of 0.07 wt.% nanocomposite are lowered slightly, compared to pure 8CB. Calculation of the splay elasticity constant from these measurements suggests that, along with dielectric anisotropy, the splay elasticity constant is also affected by the dispersion of MWCNTs. The increase does not correlate well with the dispersed amount of MWCNTs with either pristine or functionalized MWCNTs. As noted before, the nanocomposite with higher concentration of pristine MWCNTs has lower threshold voltages than pure 8CB. The functionalized MWCNT nanocomposites exhibit overall higher threshold voltages than the others, but above T - T_{NI} = -3 K, f0.07 wt.% has highest threshold voltages and below f0.007 wt.% overtakes f0.07 wt.%. This behaviour signals a subtler dependence

of MWCNT's degree of incorporation into the nematic matrix on nematic order, since birefringence or dielectric anisotropy data does not show any similar crossover.

5.2.2 Elasticity and rotational viscosities

The calculations from measured threshold voltages and dielectric anisotropies reveal that pristine MWCNTs lower the splay elastic constant, while functionalized MWCNTs increase it slightly. The difference again relates to how functionalization enables better incorporation of MWCNT dopants into the liquid crystalline matrix. The higher mechanical strength of MWCNTs is presumably better incorporated into LC matrix through $\pi - \pi$ stacking. The crossover seen in f0.07 wt.% and f0.007 wt.% threshold voltages is also present here, although it is possible to better understand it in the context of elastic energy. Presumably, f0.007 wt.% nanocomposite exhibits the highest coupling to the nematic matrix and promotes earlier onset of smectic layering as the N-SmA transition is approached. The higher rate at which splay elastic constant diverges as the transition nears coincides with the onset of smectic layering. Also, the highest birefringence increase upon nematic to smectic A transition is observed in f0.007 wt.% nanocomposite, followed by pure 8CB. f0.07 wt. %, 0.07 wt. % and 0.007 wt. % all have comparatively smaller birefringence increase upon N - Sm A transition.

Both voltage-on and voltage-off response times, over the whole nematic range, are higher compared to pure 8CB with every nanocomposite sample. For pristine MWCNT nanocomposites, voltage-on response times are twice the pure 8CB's ON response times, while voltage-off response times follow the order of dopant amount and more than twice the pure 8CB's voltage-off response time. The loss of distinction between 0.07 and 0.007 wt.% in voltage-on response suggests that multiple factors, elastic and electronic, affect the response. With functionalized samples, voltage-on and voltage-off response times of f0.07 wt.% is higher but comparatively close to 8CB. f0.007 response times are, like nonfunctionalized MWCNT nanocomposites, more than twice that of pure 8CB's. The response times of f0.007 and 0.007 wt.% nanocomposites are comparatively very close, as are the responses of pure 8CB and f0.07 wt.%.

The rotational viscosity,γ calculated from splay elastic constant and voltage-off time, yields a frame in which response times can be discussed. Pristine MWCNT nanocomposites have significantly higher rotational viscosities. It is worth noting that their rate of increase towards N-Sm A transition is different from each other and a crossover is observed here, too. The rate at which γ increases in 0.07 wt.% is similar to pure 8CB, at around 0.01 Pas/K, while 0.007 wt.% increases with 0.02 Pas/K in the middle of the nematic region. Considering that the elastic constant is lower for pristine MWCNT nanocomposites, the higher viscosity against rotation indicates a reason beyond changes in elastic energy. It is possible that MWCNTs dispersed in planar aligned nematic medium resist the bulk rotation by being anchored to nematic molecules through their shape anisotropy. The difference with which rate of γ increases as temperature drops can be understood as the effect of enhanced planar ordering on dispersed MWCNTs: As the order increases in the low concentration nanocomposite, anchoring that affects the rotation grows in strength. With higher concentration 0.07 wt.% nanocomposite, γ is higher, but lower rate of γ increase with respect to temperature suggests that the anchoring is weaker even when the dispersed amount causes slower rotation. Here, the case with functionalized MWCNTs requires more scrutiny, as f0.07 wt.% has quite low rotational viscosity, only higher than pure 8CB. f0.007 wt.%, on the other hand, has the highest rotational viscosity and the highest rate of increase of rotational viscosity ($\tilde{0}$.04 Pas/K). The better incorporation of functionalized MWCNT into nematic matrix argued by birefringence results is also supported by these results, from the perspective of above approach. This leaves f0.07 wt.%, whose behaviour can not be fully understood in the frame of explanations above and may be result of the complex interplay between disorder brought on by higher amount of MWCNTs and their interactions with nematic bulk mediated by -COOH functionalization.

5.3 Conclusion And Outlook

The results show that there are no faster response times and birefringence of nanocomposites is lowered, except for f0.007 wt.%. The only gain for all studied nanocomposites is nematic range extension. Slower responses combined with

lowered birefringence and mostly higher threshold voltages show that no significant electro-optical enhancement is brought on by MWCNT doping of 8CB in studied concentrations. However, if the irregular dependencies of quantities on concentration and functionalization are taken into account, there may be a concentration where better incorporation of MWCNTs work in the favour of electro-optical quantities of interest. A study conducted with a wide range of dopant concentrations may reveal a partial phase diagram that would be used to find the optimal amount of MWCNT for enhancing a chosen electro-optical property. Also, better understanding of MWCNT - liquid crystal interactions is needed, both experimentally and theoretically. X-ray scattering and broadband spectroscopy would be able to reveal more about intermolecular interaction between MWCNT, -COOH and 8CB. Comparisons to numerical studies would serve to analyze the findings of said experiments. This work shows that there is no straightforward way to enhance every electro-optical property of smectic 8CB at once by simply dispersing MWCNT, although functionalization serves to better incorporate MWCNT into liquid crystalline media. Only a phase diagram constructed with numerous concentrations and functionalizations might point to an optimal dopant amount.

REFERENCES

[1] **De Gennes, P.G. and Prost, J.** (1993). *The physics of liquid crystals*, 83, Oxford university press.

[2] **Blinov, L.M. and Chigrinov, V.G.** (1996). *Electrooptic effects in liquid crystal materials*, Springer Science & Business Media.

[3] **Dolgov, L.**, **Kovalchuk, O.**, **Lebovka, N.**, **Tomylko, S. and Yaroshchuk, O.** (2010). Liquid crystal dispersions of carbon nanotubes: dielectric, electro-optical and structural peculiarities, Carbon nanotubes, IntechOpen.

[4] **Stamatoiu, O.**, **Mirzaei, J.**, **Feng, X. and Hegmann, T.** (2011). Nanoparticles in liquid crystals and liquid crystalline nanoparticles, *Topics in current chemistry*, *318*, 331–93.

[5] **Zakri, C.** (2007). Carbon nanotubes and liquid crystalline phases, *Liquid Crystals Today*, *16*(1), 1–11.

[6] **Saito, R.**, **Dresselhaus, G. and Dresselhaus, M.** (2007). *Physical properties of carbon nanotubes*. 1998, Imperial College, London.

[7] **Lebovka, N.**, **Lisetski, L.**, **Goncharuk, A.**, **Minenko, S.**, **Ponevchinsky, V. and Soskin, M.** (2013). Phase transitions in smectogenic liquid crystal 4-butoxybenzylidene-4-butylaniline (BBBA) doped by multiwalled carbon nanotubes, *Phase Transitions*, *86*(5), 463–476, `https://doi.org/10.1080/01411594.2012.692091`, `https://doi.org/10.1080/01411594.2012.692091`.

[8] **Basu, R.** (2010). Dielectric studies of nanostructures and directed self-assembled nanomaterials in nematic liquid crystals, *(Ph.D. thesis)*, Worcester Polytechnic Institute.

[9] **Lebovka, N.**, **Melnyk, V.**, **Mamunya, Y.**, **Klishevich, G.**, **Goncharuk, A. and Pivovarova, N.** (2013). Low-temperature phase transformations in 4-cyano-4-pentyl-biphenyl (5CB) filled by multiwalled carbon nanotubes, *Physica E: Low-dimensional Systems and Nanostructures*, *52*, 65–69, `https://www.sciencedirect.com/science/article/pii/S1386947713000982`.

[10] **Dolgov, L.**, **Yaroshchuk, O. and Lebovka, M.** (2008). Effect of Electro-Optical Memory in Liquid Crystals Doped with Carbon Nanotubes, *Molecular Crystals and Liquid Crystals*, *496*(1), 212–229, `https://doi.`

org/10.1080/15421400802451816, https://doi.org/10.1080/15421400802451816.

[11] **Duran, H.**, **Gazdecki, B.**, **Yamashita, A. and Kyu, T.** (2005). Effect of carbon nanotubes on phase transitions of nematic liquid crystals, *Liquid Crystals*, *32*(7), 815–821, https://doi.org/10.1080/02678290500191204, https://doi.org/10.1080/02678290500191204.

[12] **Chen, H.Y. and Lee, W.** (2006). Suppression of field screening in nematic liquid crystals by carbon nanotubes, *Applied Physics Letters*, *88*(22), 222105, https://doi.org/10.1063/1.2208373, https://doi.org/10.1063/1.2208373.

[13] **Cîrtoaje, C.**, **Petrescu, E. and Moţoc, C.** (2013). Electric field effects in nematic liquid crystals doped with carbon nanotubes, *Physica E: Low-dimensional Systems and Nanostructures*, *54*, 242–246, https://www.sciencedirect.com/science/article/pii/S1386947713002464.

[14] **Singh, D.**, **Singh, U.**, **Pandey, M.**, **Dabrowski, R. and Dhar, R.** (2018). Enhancement in electro-optical parameters of nematic liquid crystalline material with SWCNTs, *Optical Materials*, *84*, 16–21, https://www.sciencedirect.com/science/article/pii/S0925346718304257.

[15] **Sigdel, K. and Iannacchione, G.** (2011). Effect of carbon nanotubes on the isotropic to nematic and the nematic to smectic-A phase transitions in liquid crystal and carbon nanotubes composites, *The European physical journal. E, Soft matter*, *34*, 1–9.

[16] **Dolgov, L.**, **Kovalchuk, O.**, **Lebovka, N.**, **Tomylko, S. and Yaroshchuk, O.**, (2010). Liquid Crystal Dispersions of Carbon Nanotubes: Dielectric, Electro-Optical and Structural Peculiarities, **J.M. Marulanda**, editor, Carbon Nanotubes, chapter 24, IntechOpen, Rijeka, https://doi.org/10.5772/39439.

[17] **Basu, R.**, **Petschek, R. and Rosenblatt, C.** (2011). Nematic electroclinic effect in a carbon-nanotube-doped achiral liquid crystal, *Physical review. E, Statistical, nonlinear, and soft matter physics*, *83*, 041707.

[18] **Vimal, T.**, **Pandey, S.**, **Gupta, S.K.**, **Singh, D.P. and Manohar, R.** (2015). Enhanced negative dielectric anisotropy and high electrical conductivity of the SWCNT doped nematic liquid crystalline material, *Journal of Molecular Liquids*, *204*, 21–26, https://www.sciencedirect.com/science/article/pii/S0167732214005285.

[19] 4 -octyl-4-biphenylcarbonitrile liquid crystal nematic, 98 52709-84-9, https://www.sigmaaldrich.com/TR/en/product/aldrich/338680.

[20] **Cacelli, I.**, **Gaetani, L.**, **Prampolini, G. and Tani, A.** (2007). Liquid Crystal Properties of the n -Alkyl-cyanobiphenyl Series from Atomistic Simulations with Ab Initio Derived Force Fields, *The journal of physical chemistry. B*, *111*, 2130–7.

[21] **Harris, P.J.**, (2004), Carbon nanotubes and related structures: new materials for the twenty-first century.

[22] **Jeon, S.Y.**, **Shin, S.H.**, **Lee, J.H.**, **Lee, S.H. and Lee, Y.H.** (2007). Effects of Carbon Nanotubes on Nematic Backflow in a Twisted Nematic Liquid-Crystal Cell, *Japanese Journal of Applied Physics*, *46*(12R), 7801, https://dx.doi.org/10.1143/JJAP.46.7801.

[23] **Dolgov**, **Yaroshchuk**, **Tomylko and Lebovka** (2012). Electro-optical memory of a nematic liquid crystal doped by multi-walled carbon nanotubes, *Condensed Matter Physics*, *15*(3), 33401, https://doi.org/10.5488%2Fcmp.15.33401.

[24] **Manjuladevi, V.**, **Gupta, R.K. and Kumar, S.** (2012). Effect of functionalized carbon nanotube on electro-optic and dielectric properties of a liquid crystal, *Journal of Molecular Liquids*, *171*, 60–63.

[25] **Lee, K.J.**, **Park, H.G.**, **Jeong, H.C.**, **Kim, D.H.**, **Seo, D.S.**, **Lee, J.W. and Moon, B.M.** (2014). Enhanced electro-optical behaviour of a liquid crystal system via multi-walled carbon nanotube doping, *Liquid Crystals*, *41*(1), 25–29, https://doi.org/10.1080/02678292.2013.829248, https://doi.org/10.1080/02678292.2013.829248.

[26] **Basu, R. and Iannacchione, G.S.** (2010). Orientational coupling enhancement in a carbon nanotube dispersed liquid crystal, *Phys. Rev. E*, *81*, 051705, https://link.aps.org/doi/10.1103/PhysRevE.81.051705.

[27] **Ganguly, P.**, **Kumar, A.**, **Tripathi, S.**, **Haranath, D. and Biradar, A.** (2014). Effect of functionalisation of carbon nanotubes on the dielectric and electro-optical properties of ferroelectric liquid crystal, *Liquid Crystals*, *41*(6), 793–799.

[28] **Neeraj, N. and Raina, K.** (2014). Multiwall carbon nanotubes doped ferroelectric liquid crystal composites: A study of modified electrical behavior, *Physica B: Condensed Matter*, *434*, 1–6.

[29] **Singh, U.B.**, **Dhar, R.**, **Dabrowski, R. and Pandey, M.B.** (2013). Influence of low concentration silver nanoparticles on the electrical and electro-optical parameters of nematic liquid crystals, *Liquid Crystals*, *40*(6), 774–782, https://doi.org/10.1080/02678292.2013.783136, https://doi.org/10.1080/02678292.2013.783136.

[30] **Basu, R.**, **Kinnamon, D. and Garvey, A.** (2016). Graphene and liquid crystal mediated interactions, *Liquid Crystals*, *43*(13-15), 2375–2390.

[31] **Lee, W.**, **Gau, J.S. and Chen, H.Y.** (2005). Electro-optical properties of planar nematic cells impregnated with carbon nanosolids, *Applied Physics B*, *81*(2-3), 171–175, https://doi.org/10.1007/s00340-005-1914-2.

[32] **Drozd-Rzoska, A.**, **Rzoska, S.J.**, **Zioło, J. and Jadżyn, J.** (2001). Quasicritical behavior of the low-frequency dielectric permittivity in the isotropic phase of liquid crystalline materials, *Phys. Rev. E*, *63*, 052701, https://link.aps.org/doi/10.1103/PhysRevE.63.052701.

[33] **Erkan, S.**, **Cetinkaya, M.**, **Yildiz, S. and Ozbek, H.** (2012). Critical behavior of a nonpolar smectogen from high-resolution birefringence measurements, *Physical review. E, Statistical, nonlinear, and soft matter physics*, *86*, 041705.

[34] **Lim, K.C. and Ho, J.T.** (1978). Coupling between Orientational and Translational Order in a Liquid Crystal, *Phys. Rev. Lett.*, *40*, 944–947, https://link.aps.org/doi/10.1103/PhysRevLett.40.944.

[35] **Lagerwall, J.**, **Scalia, G.**, **Haluska, M.**, **Dettlaff-Weglikowska, U.**, **Roth, S. and Giesselmann, F.** (2007). Nanotube Alignment Using Lyotropic Liquid Crystals, *Advanced Materials*, *19*(3), 359–364, https://onlinelibrary.wiley.com/doi/abs/10.1002/adma.200600889, https://onlinelibrary.wiley.com/doi/pdf/10.1002/adma.200600889.

[36] **Basu, R. and Iannacchione, G.** (2009). Nematic Anchoring on Carbon Nanotubes, *Applied Physics Letters*, *95*, 173113.

[37] **Baik, I.S.**, **Jeon, S.Y.**, **Lee, S.H.**, **Park, K.A.**, **Jeong, S.H.**, **An, K.H. and Lee, Y.H.** (2005). Electrical-field effect on carbon nanotubes in a twisted nematic liquid crystal cell, *Applied Physics Letters*, *87*(26), 263110, https://doi.org/10.1063/1.2158509, https://doi.org/10.1063/1.2158509.

[38] **DasGupta, S.**, **Chattopadhyay, P. and Roy, S.K.** (2001). Effect of a rigid nonpolar solute on the splay, bend elastic constants, and on rotational viscosity coefficient of $4,4^{'}-\mathrm{n}-\mathrm{octyl}-\mathrm{cyanobiphenyl}$, *Phys. Rev. E*, *63*, 041703, https://link.aps.org/doi/10.1103/PhysRevE.63.041703.

[39] **Całus, S.**, **Jabłońska, B.**, **Busch, M.**, **Rau, D.**, **Huber, P. and Kityk, A.V.** (2014). Paranematic-to-nematic ordering of a binary mixture of rodlike liquid crystals confined in cylindrical nanochannels, *Phys. Rev. E*, *89*, 062501, https://link.aps.org/doi/10.1103/PhysRevE.89.062501.

[40] **Thoen, J. and Menu, G.** (1983). Temperature Dependence of the Static Relative Permittivity of Octylcyanobiphenyl (8CB), *Molecular Crystals and Liquid Crystals*, *97*(1), 163–176,

https://doi.org/10.1080/00268948308073148, https://doi.org/10.1080/00268948308073148.

[41] **Bose, T.K.**, **Campbell, B.**, **Yagihara, S. and Thoen, J.** (1987). Dielectric-relaxation study of alkylcyanobiphenyl liquid crystals using time-domain spectroscopy, *Phys. Rev. A*, *36*, 5767–5773, https://link.aps.org/doi/10.1103/PhysRevA.36.5767.

[42] **Basu, R. and Iannacchione, G.S.** (2009). Dielectric hysteresis, relaxation dynamics, and nonvolatile memory effect in carbon nanotube dispersed liquid crystal, *Journal of applied physics*, *106*(12), 124312.

[43] **Goncharuk, A.I.**, **Lebovka, N.I.**, **Lisetski, L.N. and Minenko, S.S.** (2009). Aggregation, percolation and phase transitions in nematic liquid crystal EBBA doped with carbon nanotubes, *Journal of Physics D: Applied Physics*, *42*(16), 165411, https://doi.org/10.1088/0022-3727/42/16/165411.

[44] **Blinov, L.M.** (2010). *Structure and properties of liquid crystals*, volume123, Springer Science & Business Media.

[45] **Gruler, H. and Meier, G.** (1972). Electric Field-Induced Deformations in Oriented Liquid Crystals of the Nematic Type, *Molecular Crystals and Liquid Crystals*, *16*(4), 299–310, https://doi.org/10.1080/15421407208082793, https://doi.org/10.1080/15421407208082793.

[46] **Rahman, M. and Lee, W.** (2009). Scientific duo of carbon nanotubes and nematic liquid crystals, *Journal of Physics D: Applied Physics*, *42*(6), 063001, https://doi.org/10.1088/0022-3727/42/6/063001.

[47] **Huang, C.Y.**, **Pan, H.C. and Hsieh, C.T.** (2006). Electrooptical properties of carbon-nanotube-doped twisted nematic liquid crystal cell, *Japanese journal of applied physics*, *45*(8R), 6392.

[48] **Huang, C.Y.**, **Hu, C.Y.**, **Pan, H.C. and Lo, K.Y.** (2005). Electrooptical Responses of Carbon Nanotube-Doped Liquid Crystal Devices, *Japanese Journal of Applied Physics*, *44*(11R), 8077, https://dx.doi.org/10.1143/JJAP.44.8077.

[49] **Pandey, A.S.**, **Dhar, R.**, **Kumar, S. and Dabrowski, R.** (2011). Enhancement of the display parameters of 4'-pentyl-4-cyanobiphenyl due to the dispersion of functionalised gold nano particles, *Liquid Crystals*, *38*(1), 115–120, https://doi.org/10.1080/02678292.2010.530695, https://doi.org/10.1080/02678292.2010.530695.

CURRICULUM VITAE

Name Surname: Mehmet Can ÇETİNKAYA

EDUCATION:

- **B.Sc.:** 2010, Istanbul Technical University, Science & Letters Faculty, Physics Engineering Department
- **M.Sc.:** 2013, Istanbul Technical University, Graduate School of Science, Engineering and Technology, Physics Engineering Department

PROFESSIONAL EXPERIENCE AND REWARDS:

- 2011-2013 Researcher in BAP Project, Physics Engineering Dept., Istanbul Technical University, Istanbul, Turkey.
- 2012-2015 Research Assistant, Piri Reis University, Istanbul, Turkey.
- 7-8/2013 Visiting Student, KU Leuven, Leuven, Belgium.
- 2015-2019 Research Assistant, Istanbul Technical University, Istanbul, Turkey.
- 10-12/2018 Visiting Student by TUBITAK 2214/a Scholarship, University of Leeds, Leeds, United Kingdom.
- 2020-Current Leader R&D Test Engineer, IMTEK Cryogenics, Ankara, Turkey.

PUBLICATIONS, PRESENTATIONS AND PATENTS ON THE THESIS:

- S. Yildiz, I. Koseoglu, **M.C. Cetinkaya** 2015. Temperature-dependent electro-optical and elastic properties of carbon nanotube doped polar smectogen octylcyanobiphenyl. *Journal of Molecular Liquids*, 209(2015), 729-737.
- **M.C. Cetinkaya**, S. Yildiz, H. Ozbek 2018. The effect of -COOH functionalized carbon nanotube doping on electro-optical, thermo-optical and elastic properties of a highly polar smectic liquid crystal. *Journal of Molecular Liquids*, 272(2018), 801-814.
- Yıldız, S., **Çetinkaya, M. C.**, Özbek, H., 2019. The influence of multi-walled carbon nanotube doping on liquid crystalline phase transitions of a smectogen octylcyanobiphenyl: A high-resolution birefringence study. *Fluid Phase Equilibria*, 495(2019), 47.

OTHER PUBLICATIONS, PRESENTATIONS AND PATENTS:

- Yıldız, S., **Çetinkaya, M. C.**, Özbek, H., Tzitzios, V., Nounesis, G., 2020. High-resolution birefringence investigation on the effect of surface-functionalized CdSe nanoparticles on the phase transitions of a smectic — A liquid crystal. *Journal of Molecular Liquids*, 298 (2020), 112029.

- **Çetinkaya, M. C.**, Üstünel, Ş., Özbek, H., Yıldız, S., Thoen, J, 2018. Convincing evidence for the Halperin-Lubensky-Ma effect at the N-SmA transition in alkyloxycyanobiphenyl binary mixtures via a high-resolution birefringence study. *European Physics Journal E*, 41 (2018), 10.

  *Y*ıldız, S., **Çetinkaya, M. C.**, Üstünel, Ş., Özbek, H., Thoen, J. 2016. Test of Halperin-Lubensky-Ma crossover function at the N–Sm-A transition in liquid crystal binary mixtures via high-resolution birefringence measurements. *Physical Review E*, 93 (2016), 062706.

- Özbek, H., Üstünel, Ş., Kutlu, E., **Çetinkaya, M. C.**, 2014. A simple method to determine high-accuracy refractive indices of liquid crystals and the temperature behavior of the related optical parameters via high-resolution birefringence data. *Journal of Molecular Liquids*, 199 (2014), 275.

- **Çetinkaya, M. C.**, Yıldız, S., Özbek, H., Losada-Pérez, P., Leys, J., Thoen, J., 2013. High-resolution birefringence investigation of octylcyanobiphenyl (8CB): An upper bound on the discontinuity at the smectic- A to nematic phase transition. *Physical Review E*, 88 (2013), 042502.

- Erkan, S., **Çetinkaya, M. C.**, Yıldız, S., Özbek, H., 2012. Critical behavior of a nonpolar smectogen from high-resolution birefringence measurements. *Physical Review E*, 86 (2012), 041705.